Infrared remote temperature measurements: its physics with reference to complexities, approximations and limitations involved. I—Conceptual considerations and surface temperature estimation

RAJENDRA KUMAR GUPTA
Indian Institute of Tropical Meteorology, Pune 411 005

Received on December 20, 1977; Revised on March 13, 1978

Abstract

A nondetailing account of limitations and approximations involved in the formulation of the theory of temperature measurements by satellite exploiting the use of infrared terrestrial emission spectra is presented. Starting from spectroscopic considerations the concept of Local Thermodynamic Equilibrium (LTE), which poses altitude limitation in remote temperature measurements, is introduced towards equating the self-emission function to Planck's black body function. Surveying the emission spectra of various atmospheric gases the reasons in favour of choice for 4·3 μm and 15μ CO_2 bands are discussed. Theoretical and experimental attempts, citing the main uncertainities and limitations, for computing absorption in band/sub-bands demanded for solution of radiative transfer equation including the validity of various line shapes, the effect of time variation of CO_2 concentration and the contribution of averaging over radiometer/spectrometer filter-transmittance function/slit function towards approximations have been discussed. Estimation of sea surface temperature using 3·7 and 11 μm channels towards its estimation in cloudy conditions and the effects of *e*-type absorption arising due to dimeric water molecule formations on window region measurements and the recently reported classical statistical technique to get clear column radiance from cloudy areas have been discussed.

Key words : Physics of remote temperature measurements, Remote sea surface temperature measurements, Remote temperature measurements and clouds.

1. Introduction

The capability of space platform towards providing data over non-inhabitable regions and its enormous potential for giving data coverage on global basis resulted into compelling interests to undertake a critical study of the physics of the infrared remote temperature measurements and the retrieval of surface temperature and terrestrial temperature profile from radiance measurements. Rodgers[1] has discussed the basic methods pertaining to retrieval problem. It is proposed to present a critical review of the subject without undertaking much amplification as every aspect is a subject in itself. There is a need to know about the limitations and approximations involved in satellite-based temperature measurements in order to have a critical appreciation of the utilitative capacity of space platforms.

Remote temperature measurements could be made using active and passive methods. Accuracy in active methods to some extent could be commanded controlling the incident signal power while in case of passive sensing, mostly exploited for economic and feasibility reasons in satellite-based observations, the physical limitations are much involved in addition to engineering limitations. Here author wishes to submit the physical limitation aspects of satellite-based temperature measurements which are mostly computed rather inferred from the basic information input of infrared radiances in selected intervals. With an inclination to look into various concepts of physics involved and various assumptions effected to simplify the problem, the spectroscopic aspect of the radiative transfer problem have been attended with precision and simplicity of exposition to acknowledge the intricacies and uncertainties in the formulation of radiation transfer equation.

2. Spectroscopic considerations

The interaction of infrared emission from the lower terrestrial boundary, the earth surface, with atmosphere leads to collisional relaxation process as the scattering will be negligible except in case of shower type precipitation. Assuming linear relationship between induced emission–absorption process and density, the probability ($P_{m_1m_2}$) of molecule undergoing transition from m_1 to m_2 state after absorbing quantum of energy $h\nu_{m_1m_2}$ is given by

$$P_{m_1m_2} = \rho(\nu_{m_1m_2})\, B_{m_1m_2} \tag{1}$$

where $\rho(\nu_{m_1m_2})$, $B_{m_1m_2}$ correspond to density and Einstein absorption coefficient respectively and $B_{m_1m_2} = B_{m_2m_1}$ (Pauling and Wilson[2]). In case of spontaneous emission, its Einstein's coefficient $A_{m_1m_2}$ is given by

$$A_{m_1m_2} = \frac{8\pi h\nu^3{}_{m_1m_2}}{C^3}\, B_{m_1m_2} \tag{2}$$

The radiative interaction with electric quadrupoles and magnetic dipoles, which have respective transition probabilities 10^{-8} and 10^{-6} times that of electric dipoles, are neglected. According to Heitler[3], $B_{m_1m_2}$ and in turn $A_{m_1m_2}$, could be related to dipole moment matrix $\mu_{m_1m_2}$ by

$$B_{m_1m_2} = \frac{8\pi^3}{3\varepsilon_0 h^2}\, |\mu_{m_1m_2}|^2 \tag{3}$$

$$A_{m_1m_2} = \frac{64\pi^4 \nu^3{}_{m_1m_2}}{3\varepsilon_0 hC^3}\, |\mu_{m_1m_2}|^2 \tag{4}$$

where ε_0 is the dielectric constant.

Problem is further simplified by bifurcating Schrödinger wave equation to deal with the electronic and nuclei motions independently. The energy (E) of an isolated molecule is further assumed to be given by the linear relation

$$E = E_e + E_v + E_r + E_t + E_i$$

where E_e, E_v, E_r, E_t and E_i refer to electronic, vibrational, rotational, translational and interaction energies. Here the interaction component is further assumed small enough to permit separate treatment of electronic, vibrational and rotational spectra. Terrestrial radiations by virtue of energy considerations (Table I) can have vibrational and rotational spectra. The low energy requirement for rotational lines as compared to that for vibrational lines (Table I) leads to vibration-rotation bands. In satellite-based measurements, involving wide slit spectroscopy, band averaging is done by theoretical models because of difficulties with experimental methods and this aspect has been discussed elsewhere. Out of natural broadening, Doppler broadening, shortening of life time by collisions and molecular-molecular interactions distorting molecular energy levels (Goody[4]), the last one is unimportant under terrestrial pressure condition (Goody and Wormell[5]) while the natural broadening (Δv) using Heisenberg's uncertainty principle where $\Delta t = 1/A_{m_1m_2}$ will be

$$\Delta v = \frac{32\pi^3 v^3_{m_1m_2}}{3\varepsilon_0 hC^3} \left| \mu_{m_1m_2} \right|^2 \tag{5}$$

and as $\Delta v \alpha v^3_{m_1m_2}$, natural broadening will be unimportant in *IR* region. The self-damping is also unimportant in *IR* region.

By virtue of intramolecular forces and the time spent during collisions ($\sim 10^{-3}$ sec at S.T.P.) the phase coherence of the emitted wave trains gets destroyed as a consequence of random distribution of position (x) and velocity ($\dot{x}$). Based on Fourier analysis under the assumption that the average values of x and $\dot{x}$ after collision are zero, Lorentz arrived at the following expression for the absorption coefficient for a single j^{th} line

$$k_j(v) = \frac{S_j}{\mu} \frac{d_j(T, p)}{(v - v_j)^2 + \alpha^2}, \tag{6}$$

Table I

Spectral characteristics associated with various transitions.

Class of transition	Energy in terms of wave number	Wave length range	Classification under spectral category
Rotational	1–500 cm^{-1}	1 cm–20 μm	Microwave-far-infrared
Vibrational	500–2000 cm^{-1}	20 μm–5 μm	Infrared
Electronic	10,000 to further higher wave number in cm^{-1}	1 μm to lower wavelengths	Visible to ultraviolet

where S_j, α_j and ν_j correspond to line intensity, half width at half height and frequency at peak intensity for the j^{th} line. Equation (6) is valid when $|\nu - \nu_0| < 3M^{-1}$, where $M = 27{\cdot}8\ (C/v)^{6/5}\ b^{1/5}$, C is the velocity of light, v is the average relative velocity of the colliding molecule, and b is the constant of frequency perturbation. Here

$$\alpha_j(T, p) = \alpha_j(T_0, p_0)\left(\frac{p}{p_0}\right)\left(\frac{T_0}{T}\right)^n$$

while $S_j(T)$ is given by (Deutschman and Calfee[6])

$$S(T) = S_0\left(\frac{T_0}{T}\right)^m \exp\left[-\frac{E^1}{k}\left(\frac{T_0 - T}{T_0 T}\right)\right]$$

where E^1 corresponds to upper level and the values of α_0, S_0, n and m are experimentally determined for each line. Due to translational thermal motion of molecules the Doppler broadening, assuming equilibrium conditions and Maxwellian distribution of velocities, give rise to line shape given by (White[7] and Penner[8])

$$k(\nu) = \frac{S}{\alpha_D(T)\sqrt{\pi}}\, e^{-\frac{(\nu - \nu_0)^2}{\alpha_D^2(T)}}$$

where $\alpha_D(T)$, the Doppler half width is given by

$$\alpha_D(T) = \frac{\nu_0}{c}\left(\frac{2kT}{m}\right)^{1/2}$$

where k, m and ν_0 correspond to Boltzmann constant, mass of the molecule and wave number of the center line respectively.

The shape of the Doppler line (Fig. 1) is much narrow as compared to that for the Lorentz line as it falls of exponentially while in the case of Lorentz line the fall is inversely proportional to $(\nu - \nu_0)^2$ at wave numbers many half widths away from the centre. In case of low pressures, as in upper stratosphere, where due to large mean free path the number of collisions are less the collision broadening will be small resulting in the increased importance for Doppler broadening while in the case of high pressure the Lorentz broadening will be dominating, due to large number of collisions. On considering both Lorentz and Doppler broadening the absorption coefficient for such obtained Voigt lines, whose shape is obtained by convolution product of Lorentz and Doppler shapes (Goody[4] and Penner[8]) could be written as (Drayson[9])

$$k(\nu - \nu_0) = \frac{(ln2)^{1/2}}{\pi^{3/2}}\,\frac{S(T)}{\alpha_D(T)}\,y \int_{-\infty}^{\infty} \frac{e^{-t^2}}{y^2 + (x - t)^2}\, dt$$

where

$$y = \frac{\alpha_L(T, p)}{\alpha_D(T, p)}, \quad x = (\nu - \nu_0)\,(ln\ 2)^{1/2}\,/\alpha_D(T)$$

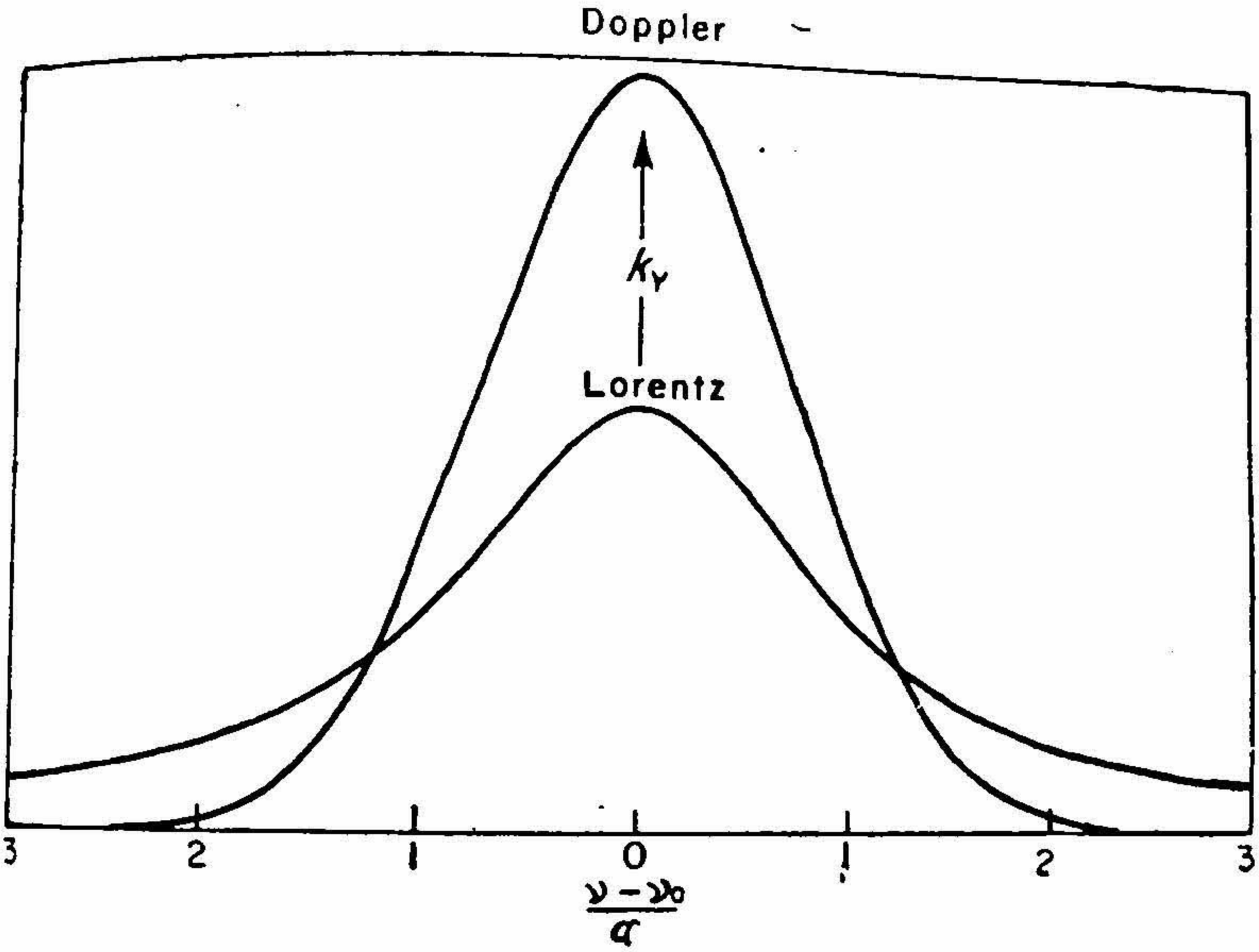

FIG. 1. Doppler and Lorentz line shapes.

and t is a dimensionless variable permitting integration over all the possible molecular velocities in the gas. - The function

$$S(T) = \int_0^\infty k(v,T)dv$$

which is independent of p will be same for Lorentz and Voigt line shapes.

Radiative transfer equation for the terrestrial atmosphere including the emission from atmosphere, by virtue of nearly same temperature range for earth and its atmosphere, based on the linear assumption of proportionality of the number of electric dipoles to interacting mass, is given by

$$-dI_\nu = [-I_\nu + f(\nu, T)]\, k_\nu\, \rho_a\, ds$$

where k_ν is the mass absorption coefficient, I_ν is the intensity of incident radiation, ρ_a is the density of the absorbing gas, dI_ν is the infinitesimal sum of change in intensity due to extinction and emission, ds is the path length and $f(\nu, T)$ is a function characterizing emission and is a function of frequency ν, temperature T, and velocity of e.m. radiation 'c'.

3. Concept of local thermodynamic equilibrium (LTE)

Under terrestrial condition, the function $f(\nu, T)$ could be equated to Planck's black body function $B[\nu, T(S)]$ provided LTE holds good even for unenclosed element case, unlike Kirchoff's law case. The statistical mechanics approach (Goody[4]), assuming that energy transfer among different spectral modes is only due to collision and considering that the Planck function could represent the unenclosed element case provided Maxwellian distribution and Boltzmann's law hold good (Milne[10]), had been used to find out the altitude limit for the validity of LTE assumption. Spitzer[11] opined the validity of Maxwell's distribution uptil stratopause while the Boltzmann's law condition was reduced by Milne[10] to the condition that the rate of deexcitation by spontaneous and radiation-induced transitions should be small as compared to the rate of deexcitation by collisions. According to Zener[12, 13] the rate of deexcitation of rotational levels is small as compared to that of the vibrational level reducing the problem to compare the rate of deexcitation of vibrational level with that of due to collisions. According to Kaplan[14] the value for the life time of CO_2 15 μm band is about $4 \cdot 10^{-1}$ second resulting in the value of rate of deexcitation equal to about 3 per second per molecule. Due to low atmospheric temperatures the effect of induced transitions in increasing the rate of deexcitation of vibrational level will not be much. The rate of deex itation due to spontaneous transitions is near about 10 per second per molecule. Henry[15] has found the value for collision efficiency in case of diatomic molecule (O_2) and it is equal to 5×10^{-6} which will be little more in case of polyatomic molecules. Assuming the value of collision efficiency to be 5×10^{-6} and same for the whole neutral atmosphere the rate of deexcitation could be calculated. Table II depicts the rate of deexcitation using the value of collision frequency as given in ARDC atmosphere[16].

While looking at Table II, it could easily be concluded that it is quite safe to assume that the rate of deexcitation by collision is higher than the rate of deexcitation due to spontaneous and radiation-induced transitions and hence at least up to stratopause the function $f(\nu, T)$ could be approximated by Planck function $B[\nu, T(s)]$, posing altitude limitation to temperature measurements, where

$$B[\nu, T(s)] = \frac{2h\nu^3}{c^2} \frac{1}{\left[\exp\left(\frac{h\nu}{kT}\right) - 1\right]}. \tag{12}$$

Here symbols have their usual meanings. Hence the radiative transfer equation could be written as

$$dI(\nu, s) = \{-I(\nu, s) + B[\nu, T(s)]\} k(\nu, s) \rho_a ds. \tag{13}$$

4. Theoretical considerations

The radiative transfer equation for a plane parallel atmosphere after converting the slant height ds in terms of vertical length dz and the angle (θ), between dz and ds

Table II

Calculation of rate of deexcitation due to collision using U.S. Standard Atmosphere[18]

Sl. No.	Altitude (in km)	Collision frequency (in Sec^{-1})	Rate of deexcitation due to collision (in per sec. per molecule) $\simeq$
1.	10	$2 \cdot 0559 \times 10^{9}$	$10 \cdot 2 \times 10^{3}$
2.	20	$4 \cdot 3546 \times 10^{8}$	$21 \cdot 7 \times 10^{2}$
3.	30	$9 \cdot 2197 \times 10^{7}$	$46 \cdot 10 \times 10$
4.	40	$2 \cdot 1037 \times 10^{7}$	$10 \cdot 52 \times 10$
5.	50	$5 \cdot 6214 \times 10^{6}$	$28 \cdot 1$
6.	60	$1 \cdot 6280 \times 10^{6}$	$8 \cdot 14$
7.	70	$4 \cdot 3174 \times 10^{5}$	$2 \cdot 15$
8.	80	$8 \cdot 94 \times 10^{4}$	$4 \cdot 5 \times 10^{-1}$

using mixing ratio for the gas (q) under the assumption $\rho \gg \rho_a$ (where ρ is the density of ambient air and ρ_a is the density of absorbing gas) which is valid in case of CO_2, and under the hydrostatic assumption could be written as

$$dI(v, \theta) = \{-I(v, \theta) + B[v, T(p)]\} k(v, p) \sec \theta \left[\frac{-q(p)}{g}\right] dp \tag{14}$$

The integration of this equation for finding out the total radiance reaching satellite in a spectral line is a matter of mathematical elegance and the equation (14) is thus normally physically integrated. As depicted in Fig. 2, the points A and C represent the position of the earth and satellite respectively while B corresponds to a particular altitude in the earth atmosphere. Let l_ν, $l_\nu + dl_\nu$ and zero be the corresponding optical path lengths between the satellite and the viewed radiances being emitted from the points A, B and C respectively. According to Beer's law

$$dI(v, \theta) = -k(v, p) I(v, 0) \left[\frac{-q(p)}{g}\right] \sec \theta \, dp \tag{15}$$

Integrating equation (15) from zero to p assuming zero pressure at satellite level we get

$$\tau(v, p, 0) = \exp\left[-\frac{1}{g} \int_0^p k(v, p) q(p) \sec \theta \, dp\right] \tag{16}$$

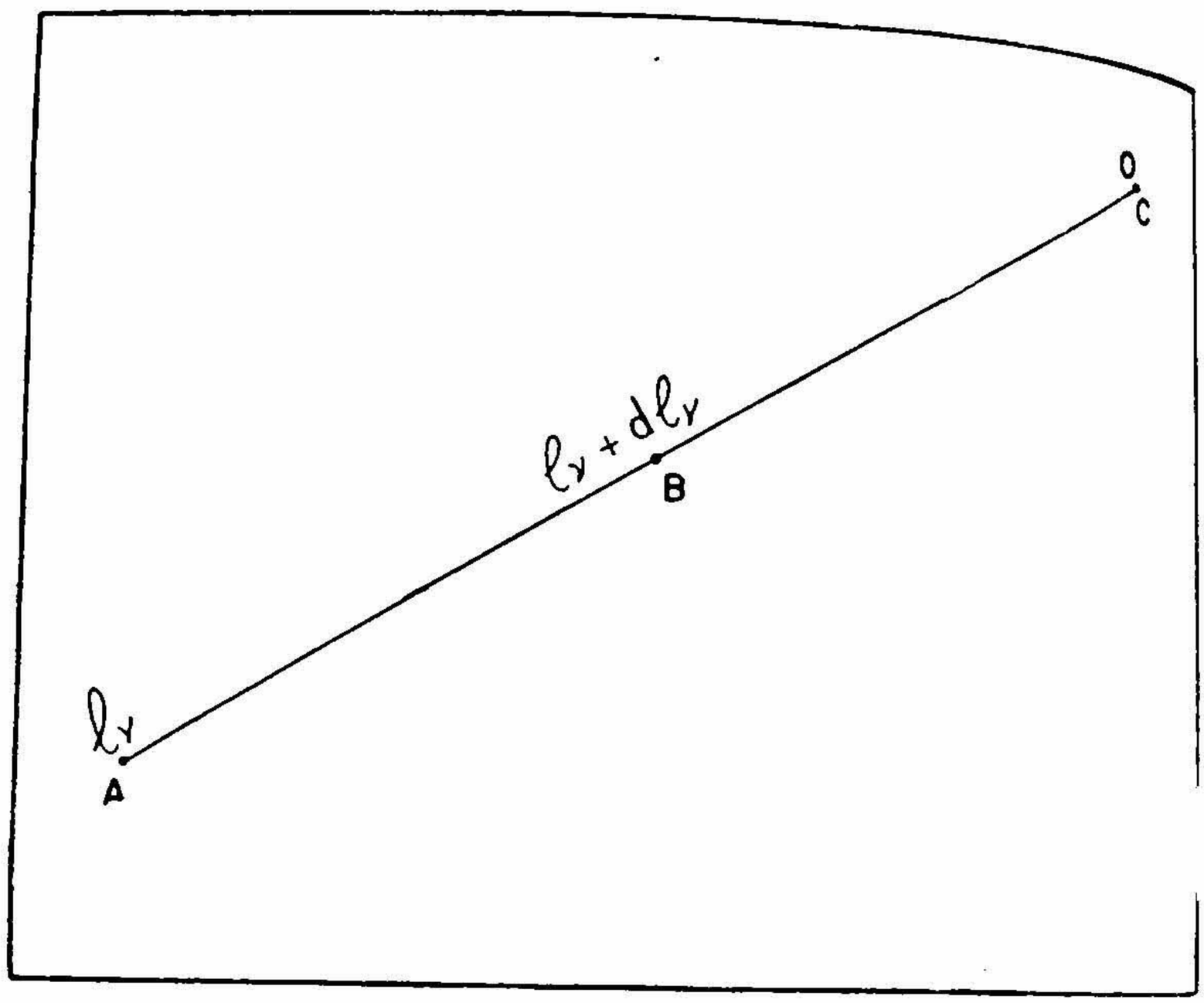

FIG. 2. Physical integration of radiative transfer equation.

where

$$\tau(\nu, p, \theta) = \frac{\{I(\nu, \theta)\}_0}{\{I(\nu, 0)\}_p}$$

is the transmittance for frequency ν from pressure level p to satellite level pressure which is assumed to be zero. On multiplying equation (16) by

$$\exp\left[-\frac{1}{g}\int_0^p k(\nu, p)\, q(p) \sec\theta \, dp\right],$$

integrating the equation so obtained from surface pressure p_s to zero to get the radiances from earth surface and the whole column of atmosphere below satellite level, equating the transmittance function at $p = 0$ to unity based on considerations of zero path length between satellite level and $p = 0$, and on the assumption of earth surface emitting as blackbody (discussed in detail by author elsewhere), we get

$$I(\nu, \theta) = B[\nu, T(p_0)]\, \tau(\nu, p_0, \theta) - \int_{p_s}^{p} B[\nu, T(p)] \frac{d\tau(\nu, p, \theta)}{dp}\, dp \qquad (17)$$

where $I[\nu, \ell]$ is the radiance received at satellite. On the right-hand side first term represents the contribution from the lower boundary modified by the transmittance function defined for, from lower boundary to satellite level while the second term speaks of the contribution from atmospheric gases participating in the process of absorption and emission modified by weighting function $d\tau(\nu, p, \ell)/dp$. Instead of coordinate p any other coordinate which is a single valued function of p could be used. The emission and absorption by the participating gas besides its spectral characteristics would be a function of its concentration and temperature only. Derr[17] and Jamieson *et al.*[18] have reviewed the molecular spectra of important atmospheric gases and following them a table conveying brief molecular-spectral characteristics of these gases with particular reference to infrared spectra has been prepared (Table III). Based on the

Table III

Table depicting infrared-microwave absorption (emission) characteristics of important atmospheric gases

Sl. No.	Participating gas	Molecular-spectral contributing characteristics of the gas	Form of spectra (with reference to information in column 3)
1	2	3	4
1.	N_2	No permanent electric dipole moment, thus no rotational and vibrational spectrum	No infrared and microwave spectrum
2.	O_2	(*a*) No permanent electric dipole moment	No infrared and microwave spectrum.
		(*b*) Magnetic moment due to interaction of electron spin and molecular angular momentum	Microwave spectrum near 60 GHz with one transition near 118 GHz
		(*c*) Combination of transitions between molecular-rotational and electron spin states	Submillimeter range extending to infrared
3.	H_2O	Asymmetric top, light, highly anharmonic with large centrifugal distortion type of molecule having much complicated spectra	Complex infrared, microwave and millimeter wavelength spectrum

Table III (*Contd.*)

1	2	3	4
4.	CO_2	Linear molecule arranged symmetrically as O C–O has no permanent dipole moment, so no pure dipole rotational spectrum	Have strong absorption in infrared
		Vibrational Modes	ν_1 mode is not active in infrared
		Electric moment change w.r. to molecular symmetry axis: None; ⊥; ∥ — O C O — Mode: ν_1, ν_2, ν_3 — Frequency (cm^{-1}): 1388, 667, 2349	
5.	CH_4	Spherical top molecule with no permanent dipole moment, thus no rotational spectra. Coriolis interactions with overtones complicate the infrared vibration spectra	Complicated infrared vibration spectra
6.	H_2	Homonuclear molecule with no dipole moment leading to no rotational spectrum. Infrared spectrum due to vibration-rotation spectrum	Vibration-rotation infrared spectra
7.	N_2O	Unsymmetrical (N–N–O) linear polyatomic molecule	Infrared and microwave spectra
8.	CO	Dipole moment exists giving rise to rotational microwave spectrum and infrared spectrum	Infrared and microwave spectra
9.	O_3	Complex rotational spectrum in infrared region	Infrared spectra

strong, not very complex, infrared absorption characteristics of CO_2, the choice for exploiting absorption-emission characteristics for remote terrestial temperature measurements goes for CO_2 gas. It is due to its being a linear symmetrically arranged molecule due to very less overlapping of absorption spectrum of other gases, and on the fact that its number density variations up to stratopause does not exceed 1% thus making the

radiance output very much less effected due to variations in mixing ratio and more or less exclusively a function of temperature. Smith[19] has discussed the energy content (relative Planck radiance), temperature sensitivity and cloud transmission characteristics in case of 4·3 μm and 15 μm bands and 5 mm band of oxygen which are given in Table IV. By looking at the energy content in a band the choice goes for 15 μm band but 15 μm band is not as sensitive as 4·3 μm band is for temperature changes in higher atmospheric temperature range which could be inferred by taking the ratio of energy emitted for 300° K and 200° K temperatures and it comes out to be 240 and 3 for 4·3 μm and 15 μm bands respectively. Looking from temperature sensitivity angle, the signal to noise ratio is good for 4·3 μm band only for temperatures near about 300° K while that for 15 μm band is satisfactory for the whole range of temperatures from 200° K to 300° K. Since the lower and upper limits of atmospheric temperature range could be considered near about 200° K and 300° K respectively, the lower temperature arising in the regions from upper troposphere to lower stratosphere could be satisfactorily recorded using 15 μm band instead of 4·3 μm band while the regions of lower troposphere and upper stratosphere could be satisfactorily recorded using 4·3 μm band instead of 15 μm band. It has been observed that using both 4·3 μm and 15 μm radiance data it is possible to construct the satellite derived temperature profile having close resemblance to temperature profile derived using radiosonde and rocketsonde data and using both channels it had been possible to resolve sharp tropopause, small vertical structures and frontal zones in the lower troposphere. A look at the last column of Table IV gives the impression that 5 mm oxygen channel is far superior to 4·3 μm and 15 μm bands in transmission through clouds but besides the technical limitations of weight and power requirements which have been overcome to some extent, the physical limitation arises because the lower boundary (Earth's surface) does not radiate as black body in 5 mm spectral region and also the emissivity of the underlying surface in case of land varies with surface structure, composition and soil moisture and in case of ocean with the height of oceanic waves. Thus the independent use

Table IV

Comparison of characteristics of 4·3 μm and 15 μm and 5 mm spectral regions (after Smith[19])

Spectral region	Energy (relative planck radiance)		Temperature sensitivity (relative to detector noise)		Cloud transmission	
	For temperature		At temperature			
	200° K	300° K	200° K	300° K	Water clouds	Ice clouds
4·3 μm	1·25	300	1	20	6%	1%
15 μm	5,000	15,000	10	6	1%	1%
5 mm	1	1	4	1	96%	99·98%

of 5 mm band is much limited but could be complementary for use with 4·3 μm and 15 μm radiance data.

During the process of emission and absorption taking place at all levels, the emission spectral lines at the lower level (in troposphere) will be broader as compared to the absorption lines at the next higher level (in troposphere) due to decrease in atmospheric temperature leading to the absorption in the centre of the line, thus the temperature information of lower levels will be contained in the wings of spectral lines. Due to increasing temperature and greater absorption towards line centre in stratospheric levels the radiance in the central parts of spectral lines will be carrying information about these levels. As the radiance emitted from lower layers will be much attenuated while the emission from upper levels will be little due to low density of the gas most of the radiance received at satellite level will correspond to intermediate levels and under such varying amount of energy the information is to be retrieved.

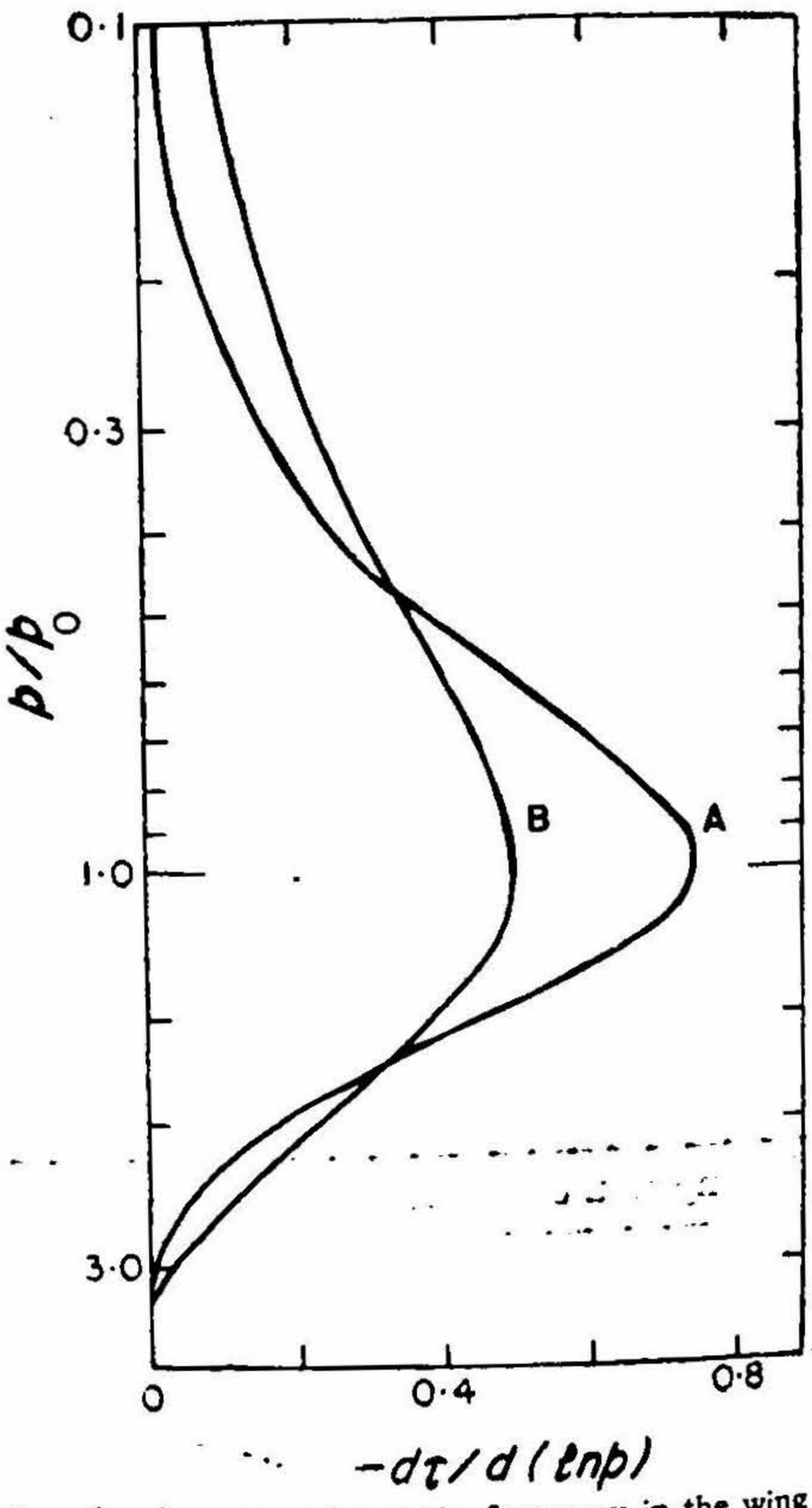

FIG. 3. Weighting functions for A, a monochromatic frequency in the wing of a collision broadened line; B, radiation received from the wings of several lines in a carbon dioxide band (after Mason[79]).

Fig. 3 depicts weighting function $-d\tau(\nu, p, \theta)/d(lnp)$ versus p/p_0 (ordinate) where p_0 refers to the pressure at which a given frequency (in case *A*) or a given spectral interval (in case *B*) will have maximum value of $-d\tau(\nu, p, \theta)/d(lnp)$ and thus Fig. 3 deals with normalised curves. It is seen that weighting function for a single collisional broadened line has less half width as compared to that for a spectral interval consisting of several lines leading to a lower vertical resolution in case of a spectral interval. As the pressure value p_0 will be different for different spectral intervals in a band due to rapid variation of absorption coefficient with frequency the plotting of weighting functions against pressure will have peaks at different altitudes as shown in Fig. 4

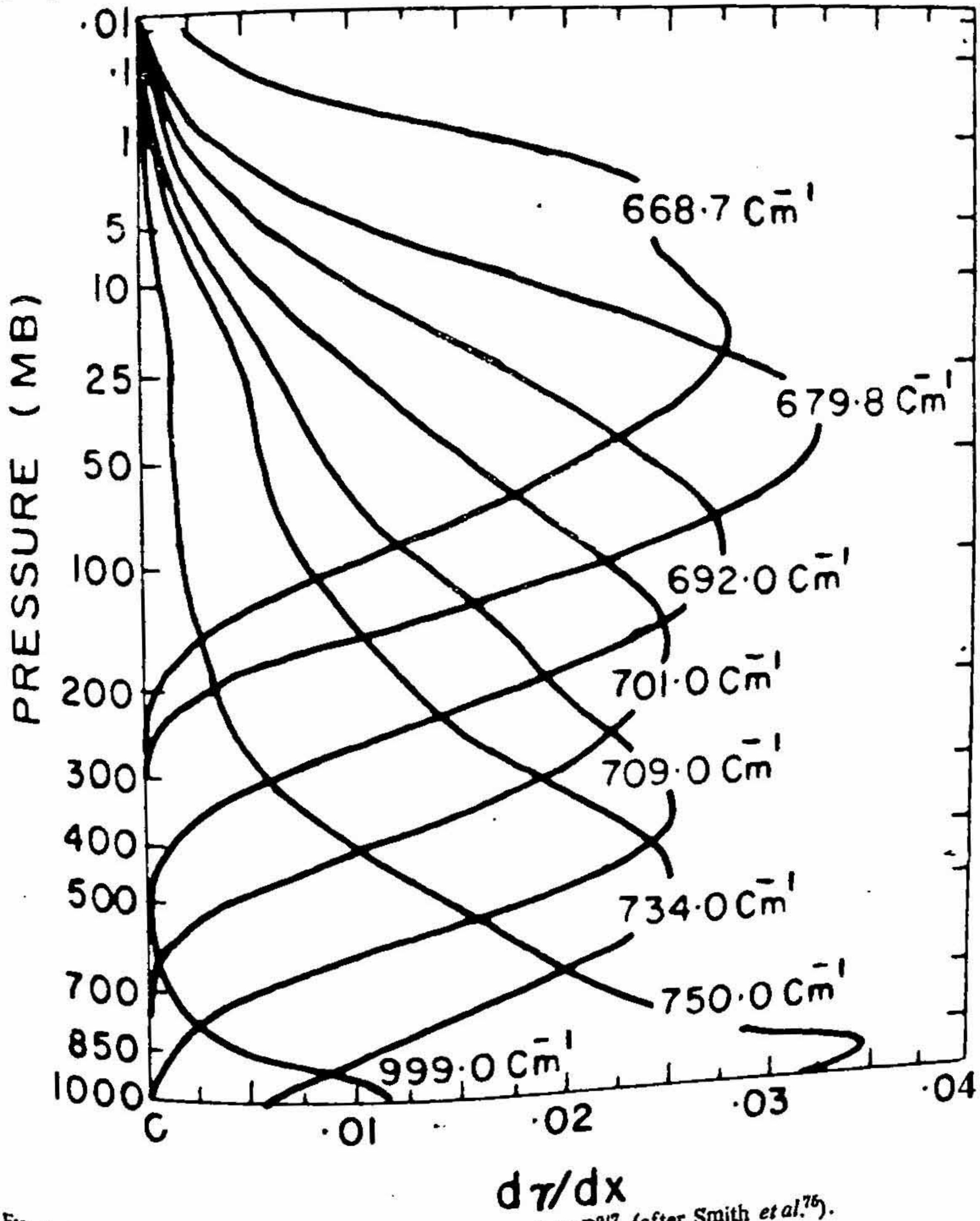

Fig. 4. Derivative of transmittance with respect to $x(p) \alpha P^{2/7}$ (after Smith *et al.*[75]).

resulting in the overlapping of weighting functions and thus the amount of radiance received in one spectral interval will not only correspond to radiation emitted from the level where its weighting function is peaking but will also be consisting of radiation emitted from other levels making the problem of retrieval of information more difficult. The weighting function could either be determined in laboratory using synthetic atmosphere or by theoretical methods using detailed spectral information regarding position, widths, intensities and shapes of the emitted spectral lines and the optical characteristics of the radiometer/spectrometer.

As infrared temperature measurement spectroscopy is essentially a wide slit spectroscopy, the determination of absorption in a band and its sub-bands by experimental methods is difficult because of difficulties encountered in simulating, within reasonable space, the continuous variation of pressure, temperature and the fractional concentration of the absorbing gas (in general) along a path in atmosphere. Experimentally only a few cells could be used in parallel for measuring absorption along the homogeneous path (constant temperature and pressure) through these cells and further difficulty is encountered in cooling of bulky synthetic atmospheric cells to atmospheric temperatures. Extrapolation of experimentally determined absorption data in a frequency interval, obtained under physical conditions (temperature, pressure, etc.) different from conditions encountered along long paths in the atmosphere, to atmospheric paths is very difficult because of complexity involved in the theoretical representation of band absorptions due to arrangements of spectral lines and their intensity distribution in a band/sub-band. This also depends on the value of frequency interval used. Averaging over a sub-band, etc. is done using theoretical models involving a good number of approximations. Except in case of very low pressures and small path lengths there are overlappings of spectral lines in a band making absorption over the band function of spacing between the spectral lines and their intensity variations, absorption being more with the increasing spacing and also more in case of equally spaced lines than in case of randomly placed lines as latter may involve much interference among lines. There are four basic models to deal with the problem under different approximations namely, Elsasser model (Elsasser[20]), Statistical model (Mayer[21], Goody[22]), Random Elsasser model (Plass[23]), and Quasi-random model (Waytt *et al.*[24]).

The estimation of absorption by a band involves the knowledge of overlapping of spectral lines which in turn need information on spacing between the spectral lines and their intensities. Obviously, other physical factors remaining the same, the absorption by a system of equally spaced spectral lines will be more than that by a system of randomly spaced spectral lines. The very rapid variation of absorption coefficient with wavelength results in the impracticability of numerical integration method leading to the choice of models involving different less realistic assumptions. Elsasser regular band model assumes that all spectral lines have same intensity and half widths and are uniformly spaced. In the statistical model random relationship of frequency centers to each other and some probability distribution function for line intensities are assumed. Spectrum in the random Elsasser model is represented by random superposition of a number of Elsasser bands having different line intensity and spacing between the lines.

It may however be noted that spacing between the spectral lines is in general neither uniform nor random. There had been difficulty in accommodating large number of weak lines, which contribute to absorption in these models. Since intensity usually decreases fairly rapidly from line to line at frequencies away from the center of the band and the earlier three models were not able to take care of it another model namely quasi-random model was developed which could represent properly the spacing among spectral lines that may occur and could simulate in a better way the intensity distribution of spectral lines including weaker lines besides representing the distribution of spectral lines in a given frequency interval in an improved way. It also included in calculation the effect of absorption due to wings of spectral lines in the neighbouring intervals. A good account of quasi-random model is available in Wyatt[24]. Elsasser model could take care of strong lines of CO_2 absorption spectrum ignoring weak lines which contribute much to the absorption over long paths while the random Elsasser model could picturise for absorption over moderate paths. In quasi-random model the absorption is first calculated over a frequency interval which is much smaller than the interval size of interest and while calculating for many spectral lines over large path length it requires much computer time. Statistical model could represent H_2O absorption over a good range of path lengths. Quasi-random model in general gives better results out of all the four models.

Kyle[25] has published an atlas of computed infrared atmospheric absorption spectra using basically McClatchey *et al.*[26] line parameter and McClatchey *et al.*[27] optical properties of mid-latitude summer profile for the vertical path through the atmosphere above altitudes of 4, 14, 30, 40, 45 and 54 km and expects that it could predict the correct atmospheric absorption within 10–20%. The basic limitations for this work had been the following :

(1) The accuracy is of $0{\cdot}01$–$0{\cdot}05\,cm^{-1}$ in spectral line frequency inputs.

(2) The accuracy is of the order of $0{\cdot}01\,cm^{-1}$ in line position shifts due to pressure.

(3) The effects of pressure induced bands and dimerization have been excluded.

(4) Variations in and temperature dependence of Lorentz half width from one spectral line to another have been approximated using mean half width value and inverse square-root dependence respectively. Computational procedures used lead to further approximation of Lorentz half width.

(5) The effect of refraction and anomalous dispersion in the vicinity of the absorption lines arising out of inhomogeneity in the atmospheric paths have been neglected.

(6) Voigt line shape which is a convolution of Lorentz and Doppler shapes has been used. Asymmetrical VanVleck-Weisskopf shape could be a better approximation for low wave number region. Many lines in 4·3 and 15 μm CO_2 bands are sub-Lorentzian. Above tropopause the effect of collisional narrowing of Doppler

half width could be significant. Rodger[28] has discussed the importance of collisional narrowing in determining the equivalent width of spectral lines. The estimation of continuum absorption in the 8–10 μm window region is limited due to uncertainties of spectral representation in the far wings of lines. Though the author does not intend to deal with remote temperature measurement exploiting microwave region, it may be mentioned that Waters[29] has reviewed well the atmospheric absorption and emission processes in this region.

Kunde and Maguire[30] have developed a direct integration transmittance model involving the computation of the monochromatic absorption spectrum by numerically summing the contributions of the individual spectral lines and have reported a disagreement of 5–10% in homogeneous path cases while in slant path cases an agreement of 5–10% in 200–2000 cm^{-1} region of emergent radiances have been reported.

Braun[31] has discussed the effect of spectral line shape and its strength and also the effect of variation of CO_2 concentration on the radiance and transmittance profiles using U.S. Standard Atmosphere Supplements[32] temperature profile for 15° N (annual) and 60° N (Winter), to represent cases of steeper and shallow lapse rates, with reference to 15 μm CO_2 band channels of Vertical Temperature Profile Radiometer (VTPR) experiment. Putting Lorentz half width as

$$\alpha_L(T, p) = \lambda \alpha_L(T_0, p_0)\left(\frac{p}{p_0}\right)\left(\frac{T_0}{T}\right)^{\gamma}$$

where λ and γ are arbitrary factors to do adjustments with $\alpha_3(T, p)$ and its temperature dependence and giving $\lambda = 1{\cdot}0$ and $\gamma = 0{\cdot}5$ values as per Drayson[33], whose line by-line integration program has been used by Braun[31], and using Lorentz line shape for $p \geqslant 100$ *mb* and Voigt line shape for $p < 100$ *mb* it was found that the uncertainties involved in transmittance profiles do not exceed the uncertainties involved in the observation process. Referring to recent Aronson *et al.*[34] measurements for few lines in the "Q" branch of ν_2 band of CO_2 mixed with N_2 over the temperature range of 200 to 300° K where they got the value of $\gamma = 0{\cdot}52$ to $1{\cdot}05$ and assuming the underestimation by 10 to 20% for γ values in Drayson's program, Braun expects at least an increase in the value of λ by 10%. Braun has calculated changes in spectral radiance for VTPR channels as a function of γ ($0{\cdot}5$ to $1{\cdot}25$) for 15° N as well as 60° N profiles keeping $\lambda = 1{\cdot}0$ and as a function of λ ($1{\cdot}0$ to $1{\cdot}8$) keeping $\gamma = 0{\cdot}5$. In both the cases carbon concentration was taken as 320 ppmv. From these it could probably be concluded that for Aronson values of γ and λ the uncertainty in calculated errors will exceed that of observations. Knowledge of correct values of γ and λ to sufficient accuracy is the basic limitation.

The global mole fraction of atmospheric CO_2 (C_{CO_2}) is 325 ± 2 ppmv (Bischof[35], Bolin and Bischof[36], and Woodwell *et al.*[37]) with an average annual rate of increase (Machta and Telegdas[38]) of

$$\frac{dC_{CO_2}}{dt} = 0{\cdot}7 \pm 0{\cdot}1 \text{ ppmv/year}$$

Additionally it also has altitudinal, latitudinal, longitudinal, secular and seasonal changes. Since the increase in CO_2 concentration will amount to increased absorption, the transmittance function peak profile will move upward with the increased concentration as in the case of increase in λ and γ. Because of steeper lapse rate at 15° N as compared to 60° N the calculated radiance changes will be more sensitive to the variations in α, γ and C_{co_2} at 15° N as compared to 60° N. To have an assessment of the consistency of transmittances, using direct integration method of Kunde and Maguire[30] and the observed radiance in Nimbus 4 Infrared Spectroscopy experiment, Kunde *et al.*[39] while examining the 550–750 cm^{-1} region, having 667 cm^{-1} CO_2 band complex as a major absorber (701 cm^{-1} O_3 band and 589 cm^{-1} N_2O band are also there in this region), for observations made over Guam and Wallops Islands, found that theoretical radiances were larger by 5–10% for 667 cm^{-1} CO_2 band. The largest deviations were observed between the 625–725 cm^{-1} region which has most of the radiation input from upper troposphere and lower stratosphere characterized by small temperature lapse rates. In their opinion due to small temperature lapse rates the calculated radiances will be insensitive to transmittance and would not be a major contributor to the observed difference.

Since satellite-based radiometers/spectrometers observe over finite band-width it becomes essential to integrate eqn. (17) over the spectral response of the instrument (Wark and Fleming[10], Fritz *et al.*[41]), to get normalised measured radiance, as follows :

$$I(\nu^*, \theta) = \frac{\int_{\nu_1}^{\nu_2} \omega(\nu^* - \nu)\ I(\nu, \theta)\, d\nu}{\int_{\nu_1}^{\nu_2} \omega(\nu^* - \nu)\, d\nu} \tag{18}$$

for spectrometer where $\omega(\nu^* - \nu)$ is the slit function and ν^* is the mean frequency of the frequency interval ν_1 to ν_2

$$I(\nu_j, 0) = \frac{\int_0^{\infty} I(\nu,\ 0)\, t(\nu_j)\, d\nu}{\int_0^{\infty} t(\nu_j)\ d\nu} \tag{19}$$

for radiometer where $t(\nu_j)$ is the filter transmittance function for the j^{th} filter and ν_j is the mean frequency corresponding to the centroid of $t(\nu_j)$.

The eqn. (18) or (19), as the case may be, is complicated one and to simplify it is assumed that over narrow spectral intervals of slit/filter transmittance function the Planck function behaviour in ν could be considered linear allowing to approximate the integration of Planck function in the spectral interval with $B[\bar{\nu}_j, T(p)]$ and $B[\bar{\nu}^*, T(p)]$ where $\bar{\nu}_j$ and $\bar{\nu}^*$ have to be properly defined frequencies depending on the frequency

response of transmittance/slit function. Additionally mean transmittance and mean weighting functions are also to be defined as follows :

$$\tau(\nu^*, p, \theta) = \frac{\int_{\nu_1}^{\nu_2} \tau(\nu, p, \theta)\, \omega(\nu^* - \nu)\, d\nu}{\int_{\nu_1}^{\nu_2} \omega(\nu^* - \nu)\, d\nu} \tag{20}$$

$$\frac{d\tau(\nu^*, p, \theta)}{dp} = \frac{\int_{\nu_1}^{\nu_2} \frac{d\tau(\nu, p, \theta)}{dp}\, \omega(\nu^* - \nu)\, d\nu}{\int_{\nu_1}^{\nu_2} \omega(\nu^* - \nu)\, d\nu} \tag{21}$$

for spectrometer and similarly for radiometer. There may be many gases, say N, participating in the process of emission and absorption in a spectral interval. Under vertical viewing conditions the transmittance functions used are approximated, assuming no systematic relation in absorption by any two gases, by

$$\tau(\nu, p, \theta) = \prod_{i=1}^{N} \tau_i(\nu, p, \theta)$$

Taking into considerations all these theoretical and physical limitations/approximations involved the equation for radiance observed at satellite could be written deleting suffixes from ν for general discussion, as

$$I(\nu, \theta) = B[\nu, T(x_0)]\, \tau(\nu, x_0, \theta) - \int_0^{x_0} B[\nu, T(x)]\, \frac{d\tau(\nu, x, \theta)}{dx}\, dx \tag{22}$$

where x is a single valued function of p. Though eqn. (22) appears similar to eqn. (17), this contains more physically realiseable quantities and various approximations.

Since carbon dioxide and oxygen are among well mixed atmospheric gases having 0·031 to 0·033% and 21% mixture by volume respectively these are used to determine atmospheric temperature structures as the emission from these will be a function of temperature only while emission bands pertaining to water vapour and ozone which are having variable mixture by volume (0–2% in case of water vapour and 0·003% in case of ozone) could be used to construct respective concentration profiles. In addition to this, atmosphere is having window regions, where absorption and emission by atmospheric constituents are negligible, in 3·5 to 4·18 μm and 10·0 to 13·0 μm regions which are used for surface and cloud temperature mappings while the window regions from 7 mm to 11 mm and greater than 15 μm could be used only for surface temperature measurements as clouds will be mostly transparent in these regions. In between 3·7 and 11 μm windows we have 6·3 μm water vapour band and 9·6 μm ozone band. In 15 μm carbon dioxide band there is little overlapping due to 13·3 μm

15·4 μm ozone band which imposes variable absorption in the 15 μm carbon dioxide band. It is experienced that an estimate of ozone profile is satisfactory for determining correction arising out of this overlapping.

5. Determination of surface temperature

The first and second terms on the r.h.s. of eqn. (22) denote contribution from lower boundary (Earth surface) and underlying atmosphere respectively. In the presence of cloud the lower boundary will be cloud while the above referred second term will represent mostly the contributions from cloud level to satellite level. Since nearly 85% of the energy contribution is from the first term its estimation becomes essential while determining temperature profile as the subtracting of lower boundary radiance contribution from the total radiance will also take care of any discontinuity which may exist in between ground temperature and air temperature at ground level. The estimation of sea surface temperature data has much importance as most of the weather takes its birth over sea. Rearranging eqn. (22) we get

$$B[\nu, T(x_0)]\,\tau(\nu, x_0, 0) = I(\nu, 0) + \int_0^{z_0} B[\nu, T(x)]\,\frac{d\tau(\nu, x, \theta)}{dx}\,dx \qquad (23)$$

The contribution of second term on r.h.s. of eqn. (23) in the window region will be very less. However it could be estimated using climatic profile or forecast profile. The limitations arising due to water vapour absorption and presence of clouds will be discussed at a later stage. As Plank function $B[\nu, T(x_0)]$ will be

$$B[\nu, T(x_0)] = \frac{c_1 \nu^3}{[\exp\,(c_2\nu/T_0) - 1]} \qquad (24)$$

where $c_1 = 2h/c^2$ and $c_2 = h/k$ and symbols have their usual meanings. Knowing $\tau(\nu, x_0, 0)$ one can find out the surface temperature by

$$T_S = \frac{c_2\nu}{\text{Log}\,[\{c_1\nu^3/B\,[\nu, T(x_0)]\} + 1]}$$

Assuming the negligible contribution from atmosphere and unity value for $\tau(\nu, x_0, \theta)$ the equivalent black body temperature (T_B) could be obtained by

$$T_B = \frac{c_2\nu}{\text{Log}\,[\{c_1\nu^3/I(\nu, \theta)\} + 1]} \qquad (25)$$

Even in the absence of clouds there will be a significant error in assuming $\tau(\nu, x_0, \theta)$ due to absorption by water vapour, a highly variable quantity particularly over the oceans where it will be increasing with the increase in surface temperature, giving rise to a temperature deficit (ΔT) in the observed value of T_B so that the corrected surface temperature (T_0) will be given by

$$T_0 = T_B + \Delta T$$

T_B will be statistically related to ΔT to a high degree due to physical reasoning discussed above. Smith and Rao[42] have depicted the relationship between ΔT and T_B the brightness temperature derived from radiance received at satellite (Fig. 5) for 3.7 μm and 11 μm window channels.

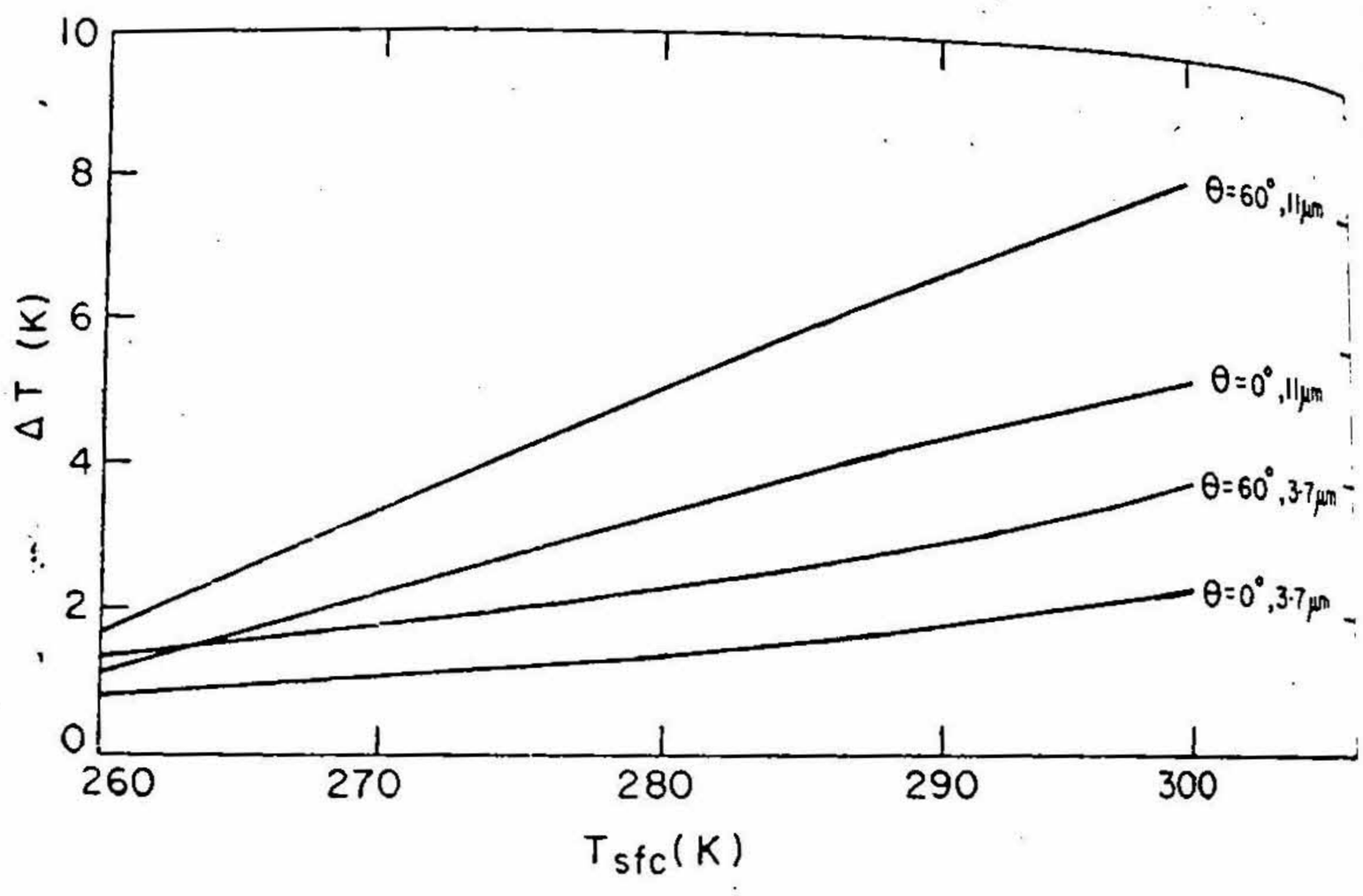

FIG. 5. Average atmospheric correction (ΔT), which must be applied to 3·7 μm and 11 μm brightness temperatures (after Smith and Rao[42]).

Following inferences could be drawn from Fig. 5.

(i) The correction (ΔT) increases with the increase in the angle of view with local vertical arising due to increased path length through water vapour.

(ii) At a given temperature, correction for 3·7 μm channel is less as compared to that for 11 μm channel the reason being due to exponential variation of Planck radiance function $B[\nu, T(p)]$ with temperature leading to a higher rate of change in radiance with temperature in 3·7 μm band as compared to that for 11 μm band. This results in maximum radiance contribution from the surface and near surface layers in 3·7 μm channel due to decrease of temperature with altitude in terrestrial atmosphere.

It may however be noted that the radiance contribution from sea surface will be from 25 to 50 μm thick skin layer while the ship measurements used to be from conventional bucket method representing the bulk temperature up to the depth of 10 cm or more. During night due to radiational cooling skin layer will be comparatively cooler by 0·5 to 1·5° K (McAlister and McLeisch[43], Ewing and McAlister[44]). As only 10% of

incoming solar energy is absorbed in the top 0·5 mm thick sea layer, McAlister and McLeisch[43] also assumed an error of the same magnitude during day. Buettner and Kern[45] experimentally studied the vertical emissivities of various materials in the 8–12 μm window region and found that in case of pure water it was 0·993 while it was 0·972 and 0·966 in cases of water plus thin film of petroleum oil and water plus thin film of corn oil respectively. Thus the approximation of sea surface emission by Planck function may cause a serious error when water surface is covered with oil and due to this reason an error could arise while comparing sea surface temperatures measured over ship with the satellite derived sea surface temperatures. Ganett *et al.*[46] reported the presence of thin films of oil over some lakes and oceans. Based on McSwain and Bernstein[47] work Buettner and Kern[45] have presented the reflectivity and emissivity of a smooth water surface as a function of inclination angle for 8·0, 11·0 and 12·5 μm wavelengths (Fig. 6) and from this it could be inferred that the deviation from black body assumption for angle of incidences $\leqslant 48^{\circ}$ for observations near 11 μm region could possibly cause an error of 0·2° K in the sea surface temperature estimation by satellites (Cogan[48]).

The absorption by water vapour is a function of its amount and partial vapour pressure (P_{H_2O}). The direct proportionality of absorption by water vapour to atmospheric humidity at the same water vapour amount were experimentally observed by Taylor and Yates[49], Streete[50] for horizontal paths and by Bignell *et al.*[51] for slant paths. McCoy *et al.*[52] measured the water vapour absorption at 25° C at the 9·5 μm and 10·59 μm CO_2 laser wavelengths and found that the absorption was proportional to the square of partial pressure of H_2O which in turn physically meant its proportionality to the amount of water vapour and its partial pressure. Dependence of this absorption on temperature have been discussed by Burch[53] in the form of Exp. (1745/T) and by Bignell[54] as -2% per degree. Absorption dependence on vapour pressure and temperature gives a thinking of a weakly bonded absorption system and the idea of absorption by dimeric water molecules [$(H_2O)_2$] was born out of these dependences. The formation of dimeric molecules could be explained by the following chemical equation:

$$2H_2O \rightleftharpoons (H_2O)_2 + \text{Binding energy}$$

The water vapour absorption coefficient (k_λ) for the parts of window region which is free of absorption lines, taking account of Burch[53] temperature dependence, could be written as

$$k_\lambda(T, p, P_{H_2O}) = k_\lambda^c P\left(\frac{T}{T_0}\right)^n + k_\lambda^{P_{H_2O}} P_{H_2O} \{\exp(1745/T)/\exp(1745/T_0)\}$$

where n could assume values in between 0·0 and 0·8 depending on the location in the rotational absorption band but usually $n = 0{\cdot}5$ (Grassl[56]) is taken in computations. Here suffix '0' refers to 0° C. Braun and Leidecker[56] treating the dimeric molecule as a symmetrical oblate top molecule, a good approximation for a simple hydrogen

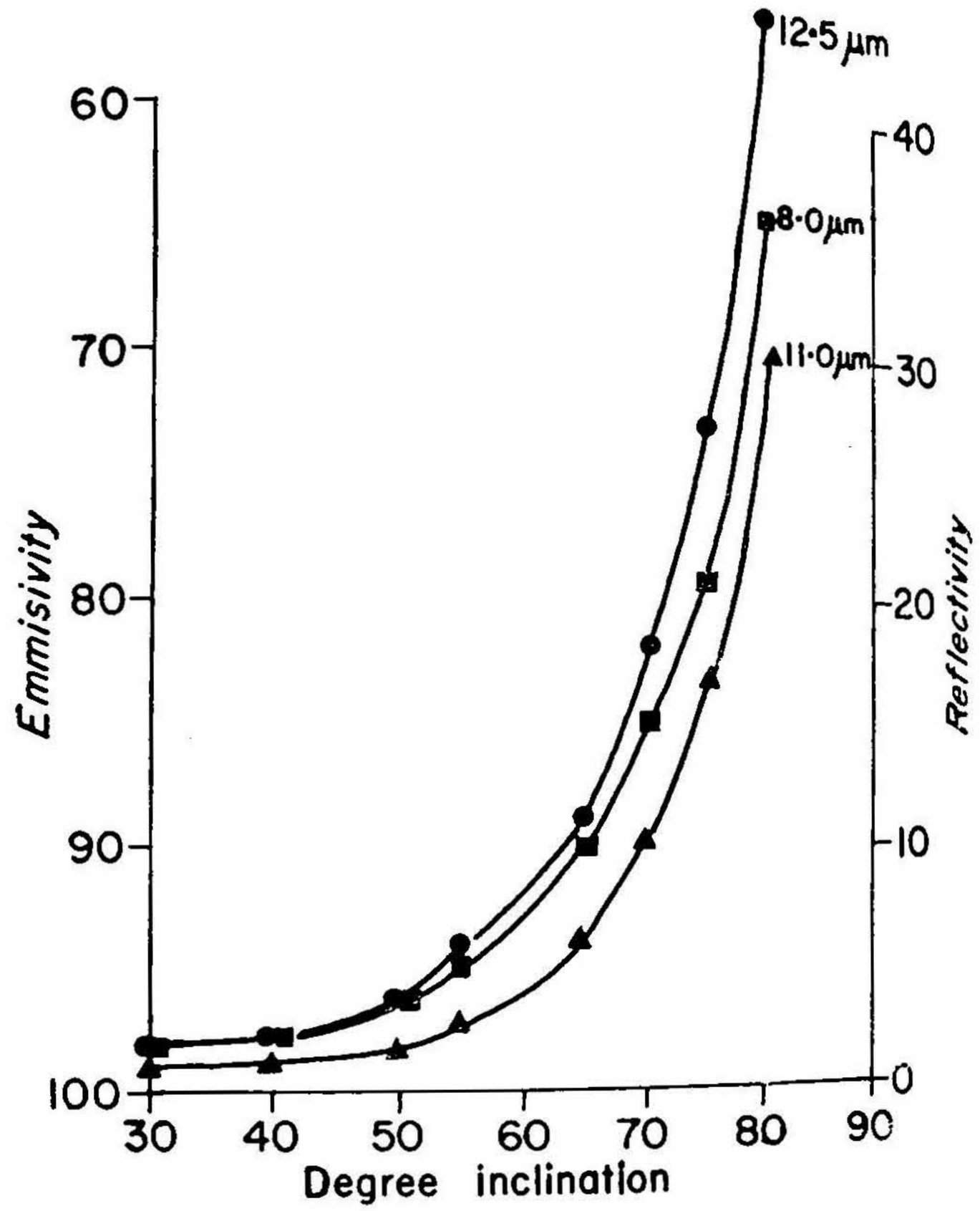

FIG. 6. Reflectivity and emissivity of a smooth water surface as a function of inclination angle for 8·0, 11·0, and 12·5 μm wavelengths (after McSwain and Bernstein[47]).

bonding case because of far heavier O-atoms which are at a distance of 3° A, estimated the binding energy of dimer molecule in the range (approximately)

$$0{\cdot}1 \text{ ev} \leqslant \text{Binding energy} \leqslant 0{\cdot}3 \text{ ev}$$

and for the window region of 8–13 μm the binding energy is found to be equal to 0·16 ev. The difference of absorption coefficient values in case of polymers as compared to these values for monomers is significant when the absorption coefficient for liquid and vapour phases are very different. It may however be noted that the maximum difference between absorptions for liquid and vapour phases occurs in the infra-

red window region. To study the $k_\lambda^{P_{H_2O}}$ dependent absorption in the 8–13 μ mwindow region Grassl[57] conducted series of measurements at Mainz. As there used to be frequent change of airmasses over the Central Europe there is nearly no correlation between relative humidity, particle density and water vapour pressure and based on this Grassl[55] separated the contribution of $k_\lambda^{P_{H_2O}}$. Fig. 7 depicts the variation of $k_\lambda^{P_{H_2O}}$ with wavelength in 8 to 13 μm range for the temperature value of 296° K. It also depicts the values of other workers and the full curve corresponds to laboratory measurements of Burch[58]. It could be inferred that for $\lambda \geqslant 10\,\mu$m there is good agreement of results of Grassl[57, 59], Burch[59] and Tomasi *et al.*[59] On the lower wavelength side the large difference appearing in Tomasi *et al.*[59] observations could arise due to comparable strong bands of N_2, CO_2 and CH_4 in the 8–9 μm region. By virtue of occurrence of peak value of terrestrial transmission in the 8–13 μm water vapour spectral window the low noise radiometric temperature measurements could be made in 11 μm channel in addition to its utility in both day and night times (discussed elsewhere). However it may be worth to mention here that the utility of this window region is restricted by the presence of strong 9·6 μm ozone band and by the Reststrahlen effect arising over deserts around 9 μm. Buettner and Kern[45] have observed a strong deviation of spectral emissivity from unity in 8–12 μm window region for all silicone materials *i.e.*, Quartz (SiO_2), Feldspar ($KAlSi_3O_8$) and Dunite (Mg_2SiO_4) which arises due to 'Reststrahlen' (residual rays) for silicon containing samples and are the effect of harmonic vibrations of the silicone oxygen bands. The desert sand is rich in

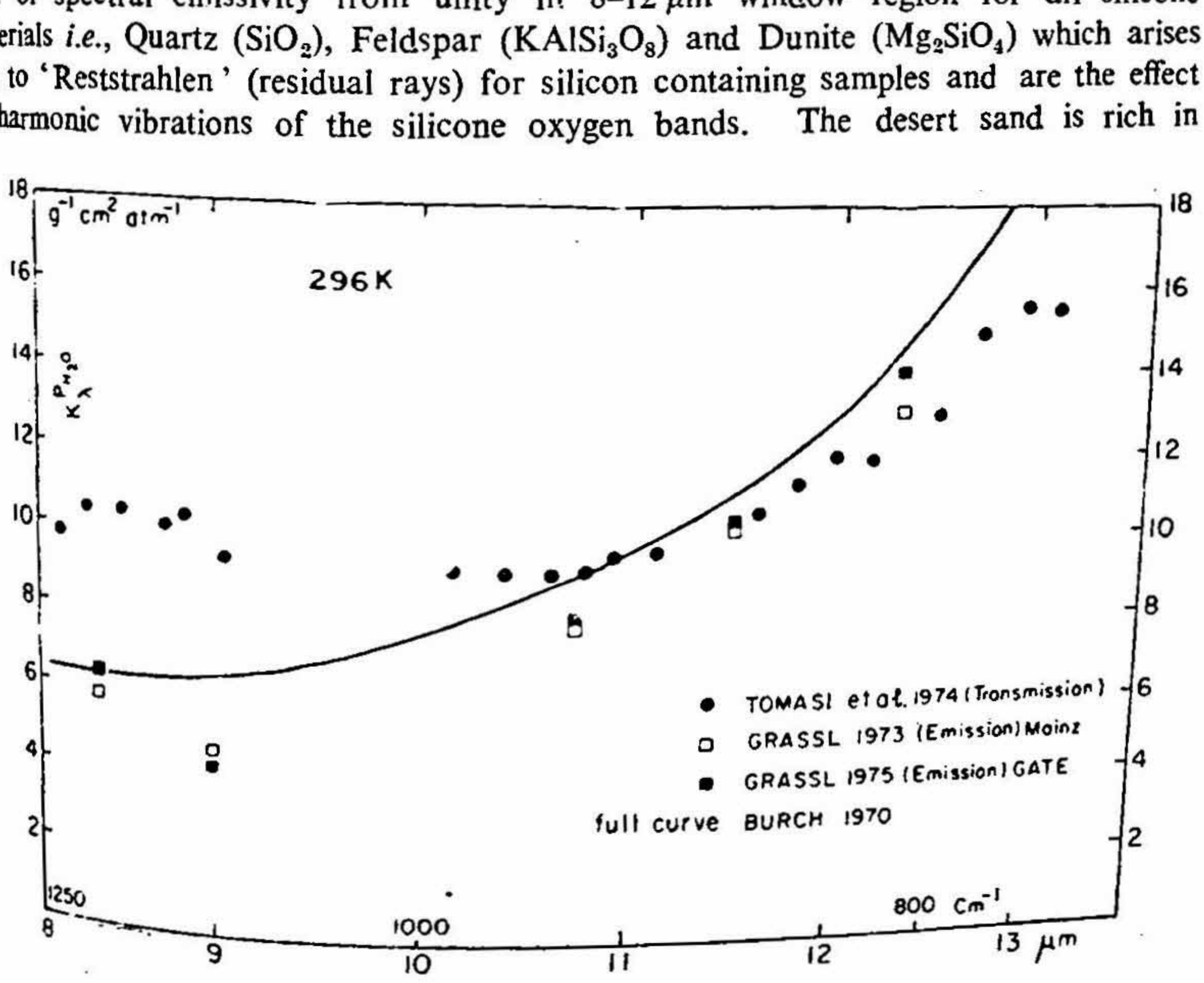

FIG. 7. Variation of $k_\lambda^{P_{H_2O}}$ with wavelength in 8 to 13 μm range (after Grassl[55]).

quartz (SiO_2) which have the strongest molecular vibrations in 9 μm spectral region and the spectral emissivity of it is a function of particle size, particle packing, background temperature and pressure. Prabhakara and Dalu[60] considering sand particle size greater than 50 μm, which makes the emissivity in 8 to 11 μm band qualitatively similar without perceptible changes in band shape, have explained, using Nimbus 4 Infrared Interferrometer Spectrometer (IRIS) measurements, the reduced emissivity over deserts which results in reduced infrared loss to space. The Reststrahlen effects due to mafic and ultramafic rocks in the 11 μm window region could not be detected by them by virtue of those being much weaker than that of quartz and due to large field of view (100 km diameter) of IRIS.

To improve the estimate of sea surface temperature the correction in 11 μm to 13 μm water vapour window region arising out of absorption by water vapour could be better determined using local vertical distribution of temperature and water vapour instead of their climatological values which may introduce an error of $\pm 2°$ K. Based on the laboratory findings about the primary dependence of water vapour absorption on its partial pressure 'e' (discussed earlier) Prabhakara *et al.*[61] have developed a transmittance model for the 775–960 cm^{-1} (12·9–10·5 μm) spectral region using Nimbus 3 and 4 Infrared Interferrometer Spectrometer (IRIS) measurements and a simple scheme which does not demand for temperature and humidity soundings but takes advantage of the differential absorption properties of water vapour in 775–960 cm^{-1} spectral region. They have modelled water vapour absorption in three spectral regions 775–831, 831–887 and 887–960 cm^{-1} to simulate the broad-band radiometer channels for the estimation of sea surface temperature and have expressed the total water vapour transmission in the 11 μm window region by

$$\tau(\nu, T) = \tau_e(\nu, T)\, \tau_p(\nu, T)\, \tau_l(\nu, T)$$

where $\tau_e(\nu, T)$ and $\tau_p(\nu, T)$ refer to transmission in the water vapour continuum while $\tau_l(\nu, T)$ refers to transmission due to water vapour lines. While dealing with water vapour lines they have assumed a statistical band model consisting of non-overlapping lines with an exponential line intensity distribution. During calculations for $\tau_e(\nu, T)$ following assumptions have been made.

(1) Assumption of exponential decrease of water vapour with altitude with a constant scale height implying the proportionality of mean water vapour pressure (e) in an atmospheric column to the total amount of precipitable water (W) in that column *i.e.*, $e = SW$, where S is constant of proportionality.

(2) Assumption rather hypothesis that for $e = 3$ mb in an atmospheric column of 1 cm^2 cross-section the value of W will be 1 gm. Thus using $e = SW$, S becomes equal to 3 mb/gm.

The $\tau_p(\nu, T)$ component assumes importance for $W < 1$ gm cm^{-2} and depends on the total pressure. Plotting total transmission at 280° K and 300° K against W (the path length of water vapour in gm/cm^2) they have found a linear relationship, as a first

approximation, among these up to 4 gm of precipitable water at both the temperatures and for all the three channels. Considering that these temperatures and path lengths cover the wide variety of atmospheric conditions from tropical to high latitudes, this linear approximation could have applicability over the whole globe. Examining six cloud free Nimbus IRIS measurements in one orbit from 8° N to 14° N along 55° E (over the Arabian Sea) of May 10, 1970, the tropical region being chosen for the reasons of large correction and its time and space variability, they found using the most transparent 10·3 to 11·3 μm channel an increase of sea surface temperature by 3° K from 8° N to 14° N. If one uses correction based on climatological information then one may consider the information to be true while using this new scheme one finds decrease in temperature by 1° K which is in agreement with seasonal pattern. They feel also that only two of the three channels are sufficient for the measurement of sea surface temperature and have shown that in cloud free regions the sea surface temperature derived through their method over 60° N to 60° S region are in agreement with the corresponding ship data, ship data being available within ± 1° of latitude and longitude, with an r.m.s. difference of 1·3° C which could also result from the error in the measurements of sea surface temperature by ships. In connection with sea surface temperature determination under Mid-Ocean Dynamic Experiment (MODE) centering near 28° N, 69° 40′ W utilizing McClatchey *et al.*[27] transmission values and computing using LOWTRAN-2 program developed by McClatchey *et al.*[27] and Selby and McClatchey[62], Cogan and Willand[63], for cloud free conditions using NOAA-2 scanning radiometer data, have developed a parameteric formula for the deficit (ΔT) in terms of integrated water vapour content and concluded that using it the sea surface temperature could be estimated with an accuracy of about ± 1° K in the MODE region within about 500 km of the subsatellite track. For the measurements in the 7·7 to 13·15 μm window region of Defence Meteorological Satellite Program (DMSP) Radiometer, having instantaneous fields-of-view of 4 and 0·6 km respectively for high and very high resolution sensors, Cogan[64, 48] has developed a parameteric formula for temperature deficit (ΔT) in the MODE region under cloud free vertical viewing conditions which in addition to parameterisation of the effect of absorption by water vapour continuum also parameterically takes care of absorption by water vapour lines and ozone. Using McClatchey *et al.*[27] distributions, the extinction contribution of aerosols had been found to be slightly less than 0·4° K while extinction contribution due to CO_2 had been numerically computed to be about 1° K and these extinction contributions had been added as constant in the final parameteric relation of ΔT with integrated water vapour content and total ozone content. With this parameteric formula, based on comparison with the limited observations, an accuracy of $\leqslant$ 1·3° K is expected by Cogan[64] over MODE region.

There had been attempts to estimate the error in surface temperature measurements arising out of absorption and reemission of surface radiance by the atmospheric constituents for cloud-free conditions in the window region. Smith *et al*[65]. did this for 3·7 μm region using model atmosphere water vapour amounts of 0·15, 1·2 and 4·7 cm as representative of polar, midlatitude and tropical atmospheres respectively to account

the effect of CO_2 and H_2O and studied the variation of this error with zenith angle. The variations for 0 to 80 degree range of zenith angle in case of polar latitudes were found to range from 0·5 to 2° K while the variations were in the ranges from 1·8 to 6·4 K and 2·7 to 11·7° K for midlatitudes and tropical latitudes respectively. At zenith angles exceeding 45° the model calculations depicted a considerable rise in error for midlatitude and tropical latitude cases. Anding and Kauth[66] using radiative transfer model (Anding and Kauth[67]) have calculated the effect of atmosphere, treating the concentration of gaseous constituents as constant while the water vapour concentration and temperature profiles were taken from model atmospheres, for five model atmospheres (Summer wet, Summer dry, Winter wet, Winter dry and mean over 30° N) three zenith angles (0°, 60° and 75°) and five ocean temperatures (280, 285, 290, 295, and 300° K). Fig. 8 depicts the upward spectral radiance at 100 km with sea temperature as a parameter for summer wet atmospheric model for the window region from which it could be inferred that atmosphere attenuates considerably in both the 9·1 and 11 μm channels. The attenuation is much in 9·1 μm channel while the attenuation in the intense absorbing regions is nearly the same for all the surface temperature values as the atmosphere is opaque in these regions. The 0° K surface temperature curve in the figure tells about the emission of the atmosphere alone.

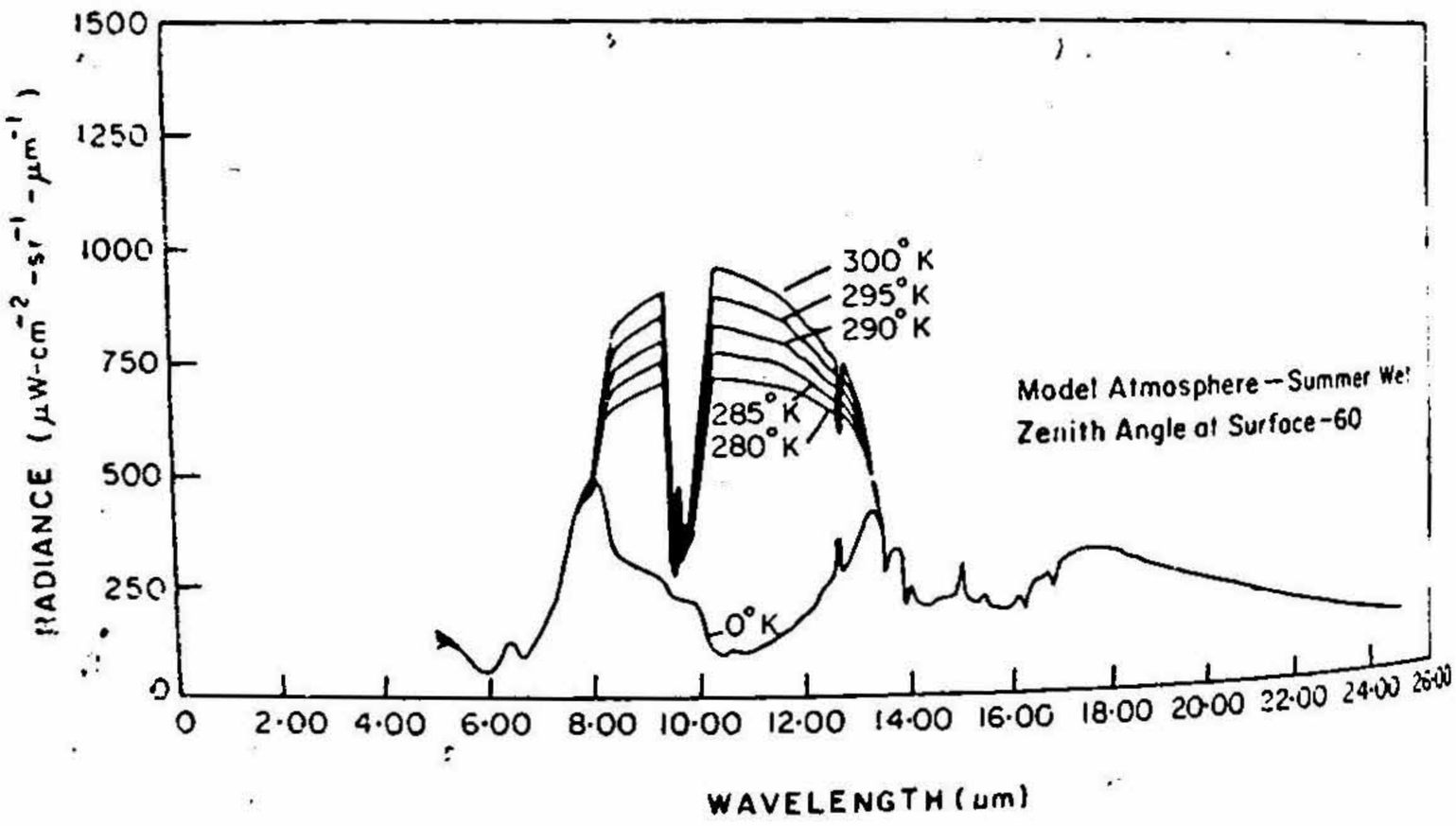

FIG. 8. Upward spectral radiance at 100 km with sea temperatures as a parameter (after Anding and Kauth[67]).

Maul and Sidran[68] studied the effect of varying atmospheric temperature profile and the effect of random noise presence in atmospheric temperature and humidity profiles. Using U.S. Standard Atmosphere[32] for January and July profiles over 30°, 45° and 60° N and annual profile over 15° N the temperature departures ΔT ($\Delta T = T_s - T_o$, where T_s

is the sea surface temperature while T_e is the calculated equivalent black body temperature), under cloud free and vertical viewing conditions, were found to be $< 2{\cdot}5°$ K in dry winter atmosphere and $> 10{\cdot}5°$ K in moist sub-tropical summer conditions. The study of the effect of random noise presence in temperature and humidity profiles, by introducing white random noise in 30° N July model atmospheric profiles, yielded an average variation in T_e within $0{\cdot}1°$ K for the introduction of $\pm$ 5% relative humidity error and standard deviation of $\pm\, 0{\cdot}7°$ K for the introduction of $\pm$ 10° K temperature error. In case of introduction of error in both relative humidity and temperature it was found that the standard deviations were larger by 30% in case of using the same series of random numbers for generating errors in both the parameters when compared to that using two independent series of random numbers.

The presence of clouds will modify the received radiance as given by eqn. (26)

$$I(\nu, \theta) = N\gamma\,(\nu, \theta)\, F(\nu, \theta) + N\varepsilon\,(\nu, 0)\, B\,[\nu, T(p_e)] + Nt\,(\nu, 0)\, B\,[\nu, T(p_0)] + (1 - N)\, B\,[\nu, T(p_0)] \tag{26}$$

where N is the fraction cloud cover, γ, ε and t are the reflectivity, emissivity and transmissivity of the cloud, suffixes 'C' and 'O' refer to cloud and surface levels and $F(\nu,\theta)$ is the amount of solar radiation energy incident on cloud. As depicted in Table V the cloud reflectivity in 11 μm and $3{\cdot}7$ μm regions are zero and 0·25 respec-

Table V

(*After Smith and Rao*[42])

Spectral band	N	r	ε	t	B_ν [200° K]	B_ν [300° K]	I_ν	T_B
11 μm	0·5	0	1	0	13·413	117·46	65·438	265° K
3·7 μm	0·5	0·25	0·75	0	0·0009	0·5579	0·2793	285° K

tively reducing the contribution of solar radiation energy to observed radiance zero in 11 μm channel while in $3{\cdot}7$ μm channel where radiance due to solar radiation is quite comparable to terrestrial radiation, the reason which makes it much useful only in night time, its contribution to observed radiance is significant. Assuming clouds to be opaque Smith and Rao[42] have estimated surface temperature based on the assumption of 50% cloud cover, cloud and surface temperatures being at 200° K and 300° K respectively (Table V) and have arrived at the figures of 265° K and 285° K for surface temperature T_B in 11 μm and $3{\cdot}7$ μm channels respectively. Though $3{\cdot}7$ μm channel gives better estimate, it could be used only for night time for the reason discussed

earlier. Utilizing same values for cloud characteristics (as shown in Table V) and using 250° K and 290° K as cloud and surface temperatures respectively they have derived the variation of ΔT with cloud amount for both channels as shown in Fig. 9. Since the rate of variation of Planck radiance with temperature is very different in 3·7 μm and 11 μm bands, measurements of both could be used to determine sea surface temperature in the presence of clouds. Maul and Sidran[68] studying the effect of cloud cover and cloud height on sea surface temperature measurements using 30° N July U.S. Standard Atmosphere[32] temperature profiles found that for the same atmospheric state and cloud coverage percentage the errors were large for large value of sea surface temperatures. For a given cloud coverage, the error due to cloud height was found to be more for increasing cloud heights in the field of view. A towering cumuloform cloud occupying 10% field of view at 8 km altitude introduced an error of 4° K while for the same per cent of cloud coverage at 1 km the error would be of 0·5° K. An error of < 1° K had been anticipated for fracto-cumulus clouds at < 2 km altitude. Using classical standard technique (Cohen[69,70] and Halperin[71]) Crosby[72] has developed

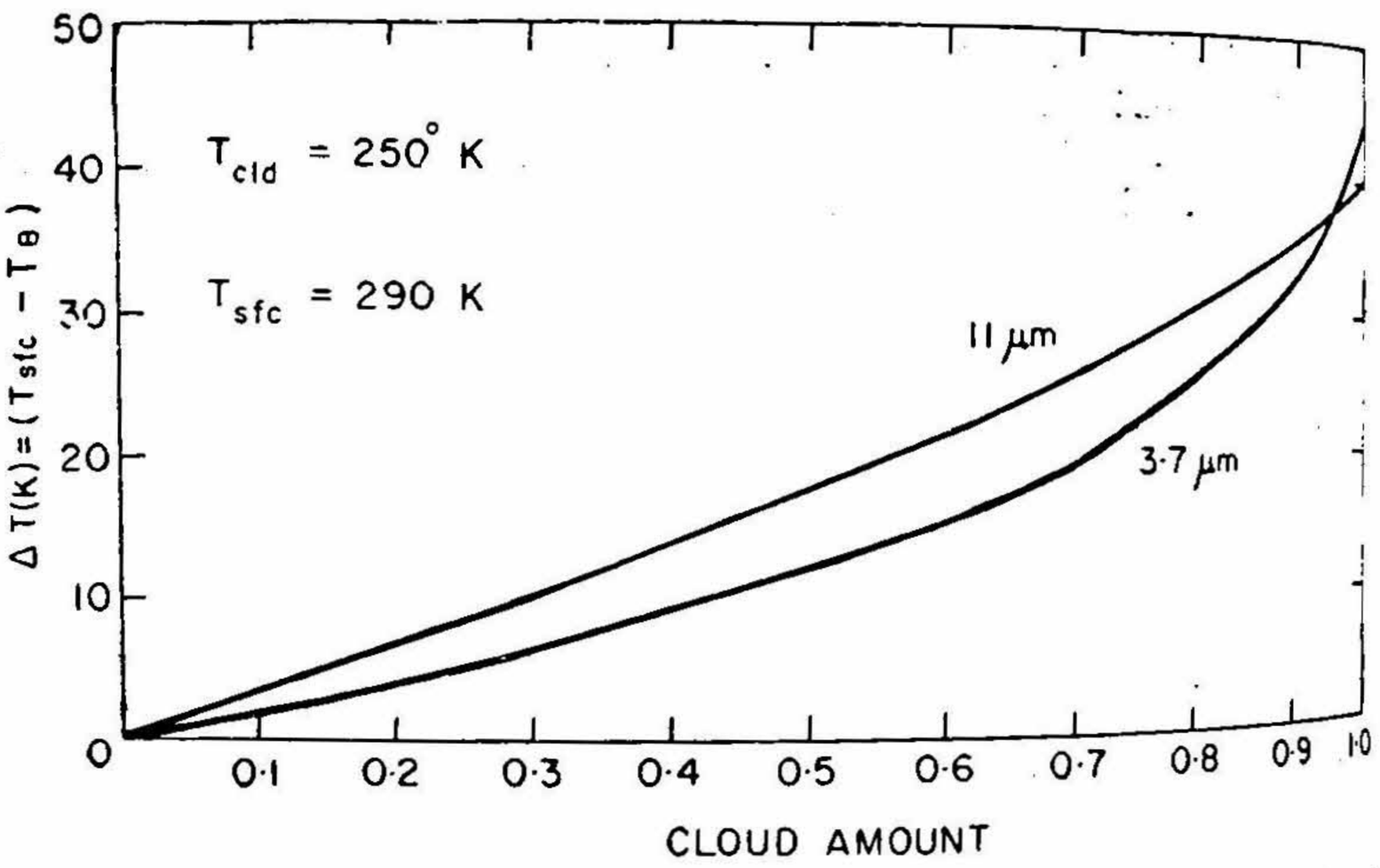

FIG. 9. Difference between 3·7 μm and 11 μm brightness temperature and surface temperature as a function of cloud amount (after Smith and Rao[42]).

a statistical technique for getting clear column radiances for surface temperature measurement from cloudy areas under the assumptions that (1) There are a number of neighbouring measurements where radiances in the absence of clouds would be the same, (2) The presence of clouds lowers the radiance, (3) Some of the fields of view are cloud free, and (4) The difference between radiances from two cloud free fields of view is due only to instrument noise whose distribution is assumed normal with known standard

deviation. The probability density function $h(\gamma)$ for the large number of neighbouring radiance measurements under the earlier mentioned assumptions could be modelled as

$$h(\gamma) = (1 - \alpha)\ g(\gamma) + \alpha f(\gamma)$$

where $g(\gamma)$ and $f(\gamma)$ refer to probability density for cloudy and clear areas respectively while 'α' refers to the proportion of clear fields of view. $f(\gamma)$ as per assumption (4) is given by

$$f(\gamma) = \frac{1}{2\pi\sigma} \exp\left[-(\gamma - \mu)^2/2\sigma^2\right]$$

where μ corresponds to radiance from cloud free field of view in the absence of noise γ the observed radiances and σ the standard deviation. The $h(\gamma)$ expression could be simplified taking a value T such that $g(\gamma) \to 0$ for $\gamma > T$ and assuming a value of $\alpha \geqslant m/n$ where m refers to the number of the largest measured radiances out of tota number of n measured radiances and under such conditions the estimate of clear column radiance contained in the tail of $h(\gamma)$ could be obtained from the maximum likelihood estimate of μ from the normalized tail of $h(\gamma)$ by

$$P(y) = \frac{\exp - \left[(y - \mu)^2 + 2\sigma^2\right]}{\int_T^\infty \exp - \left[(t - \mu)^2/2\sigma^2\right] dt}, \quad y > t$$

where $P(y)$ refers to the tail of $h(\gamma)$. By changing the variable y and μ by

$$x = \frac{y - T}{\sigma}$$

and

$$W = -\left(\frac{\mu - T}{\sigma}\right)$$

and solving the above equation for the maximum likelihood estimate of W, *i.e.*, W one gets

$$-\hat{W} + \frac{\exp(-\hat{W}^2/2)}{\int_{\hat{w}}^\infty \exp(-V^2/2)\, dv} = \bar{X}$$

where

$$V = \frac{t - T}{\sigma} \quad \text{and} \quad \bar{X} = \frac{1}{n} \sum_{i=1}^{n} Xi$$

Deciding about truncation value T one could first select the highest m_1 (say 100) radiances out of n (say 1000) assigning minimum boundary value of this m_1 group to T.

Calculating $\bar{X}_{m_1}$ for this group μ_{m_1} could be estimated. Similarly selecting maximum m_2 (say 200) values again $\bar{X}_{m_2}$ and μ_{m_2} could be calculated. To decide about the criteria of μ_{m_2} as a good estimate of clear radiance the following conditions need to be satisfied.

$$(\mu_{m_2} - T) > 1\sigma \text{ and } (\mu_{m_1} - \mu_{m_2}) < 0{\cdot}2\sigma$$

If $(\mu_{m_2} - T) > 1\sigma$ then the process of selecting highest m_3 (say 300) and doing calculations as referred above are continued till the above written conditions are satisfied. If $(\mu_{m_2} - T) > 1\sigma$ and $(\mu_{m_1} - \mu_{m_2}) > 0{\cdot}2\sigma$ then it is concluded that the field is too much contaminated with clouds and the set is rejected. Applying the technique to radiance measurements in 10·5–12·5 μm scanning radiometer data, Crosby and DePriest[73] opine that by virtue of the requirement of much smaller percentage of clear areas as compared to that for other operational methods this new technique provides at least a 10% more yield of retrieved clear column surface radiances. Using the night time scanning radiometer visible data as pure noise, Crosby and DePriest have shown that new technique could have more than 99% yield with a bias of 0·02 counts and a standard deviation of 0·39 counts while the yield of operational technique has been 75% with a bias of 0·21 counts and a standard deviation of 0·89 counts.

6. Conclusion

The author has attempted to present a cohesive picture of the wider details of the subject of passive remote temperature measurement physics and of the surface temperature estimation aspect specifically over the oceans where it is difficult to get data by conventional methods. Recently attempts are being made to ascertain the non-LTE temperature using coupled $\nu_1\nu_2$ modes of CO_2 vibrational temperature in 15 μm band (Kumer[74]) which may be useful in overcoming the altitude limitation in satellite-based remote temperature measurements.

7. Acknowledgements

The author is thankful to Mr. M. H. Gangawane for the pains taken in typing the manuscript and to Mr. Brij Mohan for his unique help in comparing the manuscript with the typed material. The author is profoundly grateful to the Director, Indian Institute of Tropical Meteorology, Pune, for permitting the publication of this manuscript.

References

1. Rodgers, C. D. Retrieval of atmospheric temperature and composition from remote measurements of thermal radiation. *Revs. Geophys. and Space Phys.*, 1976, **14**, 609–624.

2. PAULING, L. AND WILSON, E. B. — *Introduction to Quantum Mechanics*, 1935, McGraw-Hill Book Company, New York.

3. HEITLER, W. — *The Quantum Theory of Radiation*, 1960, Clarendon Press, Oxford.

4. GOODY, R. M. — *The Physics of Stratosphere*, 1954, Cambridge University Press.

5. GOODY, R. M. AND WORMELL, T. W. — The quantitative determination of atmospheric gases by infrared methods I. Laboratory determination of the absorption of the 7·8 and 8·6 μm bands of nitrous oxide with dry air as a foreign gas. *Proc. Royal Socy.*, 1951, 209A, 178–196.

6. DEUTSCHMAN, E. M. AND CALFEE, R. F. — Two computer programs to produce theoretical absorption spectra of water vapour and carbon dioxide, U.S. Department of Commerce, National Bureau of Standards, 1967, Tech. Note 332.

7. WHITE, H. E. — *Introduction to Atomic Spectra*, 1934, McGraw-Hill Book Company, Inc., New York.

8. PENNER, S. S. — *Quantitative Molecular Spectroscopy and Gas Emissivities*, 1959, Addison-Wesley Publishing Company, Inc., Reading, Mass.

9. DRAYSON, S. R. — Atmospheric transmission in the CO_2 bands between 12 and 18 μm. *Applied Optics*, 1966, pp. 385–391.

10. MILNE, E. A. — *Handbuch der Astrophysik*, 1930, Springer, Berlin.

11. SPITZER, L. — *The Atmosphere of the Earth and Planets*, 1949, Chicago University Press.

12. ZENER, C. — Interchange of translational, rotational and vibrational energy in molecular collisions, *Phys. Revs.*, 1931, 37, 556–569.

13. ZENER, C. — Low velocity inelastic collisions. *Phys. Revs.*, 1931, 38, 227–281.

14. KAPLAN, L. D. — Line intensities and absorption for the 15 micron carbon dioxide band, *J. Chem. Phys.*, 1950, 18, 186.

15. HENRY, P. S. H. — The energy exchange between molecules, *Proc. Cambridge Phil. Socy.*, 1932, 28, 249–255.

16. — *U.S. Standard Atmosphere*, 1962, U.S. Government Printing Office, Washington D.C.

17. DERR, V. E. — The spectra of molecules of the Earth's atmosphere, In *Remote Sensing of Troposphere*, edited by V. E. Derr, Ch. 9, 1972, National Oceanic and Atmospheric Administration and University of Colorado, Colorado.

18. JAMIESON, J. A., MCFEE, R. H., PLASS, G. N., GRUBE, R. H. AND RICHARDS, R. B. — *Infrared Physics and Engineering*, 1963, McGraw-Hill Book Company, New York.

19. SMITH, W. L. — Satellite techniques for observing the temperature structure of the atmosphere. *Bull. Amer. Meteorol. Socy.*, 1972, 53, 1074–1082.

20. ELSASSER, W. M. — Mean absorption and equivalent absorption coefficient of a band spectrum, *Phys. Revs.*, 1938, **54**, 126–129.

21. MAYER, H. — *Methods of Opacity Calculations*, 1947, Los Alamos, LA-647

22. GOODY, R. M. — A statistical model for water vapour absorption. *Quart. J. Roy. Meteorol. Socy.*, 1952, **78**, 165–169.

23. PLASS, G. N. — Models for spectral band absorption, *J. Optical Socy. Amer.*, 1958, **48**, 690–703.

24. WYATT, P. J., STULL, V. B. AND PLASS, G. N. — Quasi-random model of band absorption, *J. Optical Socy. Amer.*, 1962, **52**, 1209–1217.

25. KYLE, T. G. — Atlas of computed infrared atmospheric absorption spectra, *NCAR Tech Note*, 1975, NCAR-TN/STR-112, 72 p.

26. MCCLATCHEY, R. A., BENEDICT, W. S., CLOUGH, S. A., BURCH, D. E., CLAFEE, R. F., FOX, K., ROTHMAN, L. S. AND GARING, J. S. — AFCRL atmospheric absorption line parameters compilation, AFCRL-TR-73–0096, Environmental Research Paper No. 434, 1973, Air Force Cambridge Research Laboratories, Bedford, Mass, 78 p.

27. MCCLATCHEY, R. A., FENN, R. W., SELBY, J. E. A., VOLZ, F. E. AND GARING, J. S. — *Optical Properties of the Atmosphere*, (Third edn.), AFCRL-72–0497, Environmental Research Paper no. 411, 1972, Air Force Cambridge Research Laboratories, Bedford, Mass, 108 p.

28. RODGERS, C. D. — Collisional narrowing : its effect on the equivalent width of spectral lines, *Applied Optics*, 1976, **15**, 714–716.

29. WATERS, J. W. — Absorption and Emission by Atmospheric Gases, 1976, In *Methods of Experimental Physics*, Vol. 12, *Astrophysics*, Part B, Radio Telescopes, 142–176, Academic Press, Inc., New York.

30. KUNDE, V. G. AND MAUGIRE, W. C. — Direct integration transmittance model, *J. Quant. Spectrosc. Radiat. Transfer*, 1974, **14**, 803–813.

31. BRAUN, C. — *Dependence of VTPR Transmittance Profiles and Observed radiances on Spectral Lines Shape Parameters*, NOAA NESS 70, 1975, National Oceanic and Atmospheric Administration, Washington, D.C.

32. — United States Standard Atmosphere Supplements prepared by National Oceanic and Atmospheric Administration, National Aeronautics and Space Administration and United States Air Force, 1966, Supdt. of Documents, Govt. Printing Office, Washington DC, 289 p.

33. DRAYSON, S. R. — Atmospheric transmission in the CO_2 bands between 12 and 18 μm, *Applied Optics*, 1966, **5**, 385–391.

34. ARONSON, J. R., VON THUNA, P. C., AND BUTLER, J. E. — Tunable diode laser high resolution measurements of the ν_3 vibration of CO_2, Final Report ADL C-76028, 1974, A.D. Little Inc., Cambridge, Mass 02140, NOAA Contract 3-35384, 41 p.

35. BISCHOF, W. — Carbon dioxide concentration in the upper troposphere and lower stratosphere III, *Tellus*, 1963, 25, 305–308.

36. BOLIN, B. AND BISCHOF, W. — Variations of the carbon dioxide content of the atmosphere in the Northern Hemisphere, *Tellus*, 1970, 32, 431–442.

37. WOODWELL, G. M., HOUGHTON, R. A. AND TEMPEL, N. R. — Atmospheric carbon dioxide at Brookhaven: patterns of variation up to 125 meters, *J. of Geophys. Res.*, 1973, 78, 932–940.

38. MACHTA, L. AND TELEDAS, K. — Inadvertent large scale weather modification. In *Weather and Climate Modifications*, edited by W. N. Hess, 1974, J. Wiley and Sons, New York.

39. KUNDE, V. G., CONRATH, B. J., HANEL, R. A., MAGUIRE, W. C., PRABHAKARA, C. AND SALOMONSON, V. V. — The Nimbus 4 infrared spectroscopy experiment 2. Comparison of observed and theoretical radiances from 425–1450 cm^{-1}, *J. Geophys. Res.*, 1974, 79, 777–784.

40. WARK, D. Q. AND FLEMING, H. E. — Indirect measurements of atmospheric temperature profiles from satellite 1. Introduction. *Mon. Wea. Rev.*, 1966, 94, 351–362.

41. FRITZ, S., WARK, D. Q., FLEMING, H. E., SMITH, W. L., JACOBOWITZ, H., HILLEARY, D. T. AND ALIHOUSE, J. C. — Temperature sounding from satellites, NOAA TR NESS 59, National Oceanic and Atmospheric Administration, Washington, D.C., 1972, 49 p.

42. SMITH, W. L. AND RAO, P. K. — The determination of surface temperature from satellite 'window' radiation temperature measurements, *Proceedings of the Fifth Symposium on Temperature*, Washington D.C., June 21–24. 1971, p. 2251.

43. MCALISTER, E. D. AND MCLEISCH, W. — Heat transfer in the top millimeter of the ocean, *J. Geophys. Res.*, 1969, 74, 3408–3414.

44. EWING, G. C. AND MCALISTER, E. D. — On the thermal boundary layer of the ocean. *Science*, 1960, 131, 1374–1376.

45. BUETTNER, K. J. K. AND KERN, C. D. — The determination of infrared emissivity of terrestrial surfaces, *J. Geophys. Res.*, 1965, 70, 1329–1337.

46. GARRETT, W. D., TIMMONS, C. O., JARVIS, N. L. AND KAGARISE, R. E. — *Constitution and Surface Chemical Properties of Sea Slicks*, U.S. Naval Research Laboratory, Washington, D.C., 1963.

47. MCSWAIN, B. AND BERNSTEIN, J. — Specular reflectance of water in the 1·5 to 15-micron region as a function of wavelength and incidence angle, Navwets Report 7162, *Quarterly Report*, 1960, Foundational Research Project, October–December, 1960.

48. COGAN, J. L — Interpretation and utilization of satellite measurements of sea surface temperature, *Ph.D. Thesis*, Imperial College of Science and Technology, University of London, 1972. 103 p.

49. TAYLOR, J. H. AND YATES, H. W. — Atmospheric transmission in the infrared, *J. Optical Socy. Amer.* 1957, 47, 223–226.

50. STREETE, J. L. — Infrared measurements of atmospheric transmission at sea level, *Applied Optics*, 1968, 7, 1545–1549.

51. BIGNELL, K. J., SAIEDY, F. AND SHEPPARD, P. A. — On the atmospheric infrared continuum, *J. Optical Socy. Amer.*, 1963, 53, 466–479.

52. MCCOY, J. H., RENSCH, D. B. AND LONG, R. K. — Water vapour continuum absorption of carbon dioxide laser radiation near 10 μm, *Applied Optics*, 1969, 8, 1471–1478.

53. BURCH, D. E. — *Investigation of the Absorption of Infrared Radiation by Atmospheric Gases*, Semi-annual technical report, contract no. F 19628-69–C-0263, Philcc-Ford Corporatien, Newport Beach, California, 1970.

54. BIGNELL, K. J. — The water-vapour infrared continuum, *Quart. Journ. Royl Meteorol. Socy.*, 1970, **96**, 390–403.

55. GRASSL, H. — A new type of absorption in the atmospheric infrared window due to water vapour molecules, *Contributions to Atmospheric Physics*, 1976, 49, 226–236.

56. BRAUN, C. AND LEIDECKER, H. — Rotation and vibration spectra for the H_2O dimer: Theory and comparison with experimental data, *J. Chem. Physics*, 1974, 61, 3104–3113.

57. GRASSL, H. — Separation of atmospheric absorbers in the 8–13 micrometer region, *Contributions to Atmospheric Physics*, 1973, 46, 75–81.

58. GRASSL, H. — *e*-type absorption in tropics, Global Atlantic Tropical Experiment Report 14, *World Meteorological Organisation* and *International Council of Scientific Unions*, 1975, 1, 298–303.

59. TOMASI, C., GUZZI, R. AND VITTORI, O. — A search for the *e*-effect in the water vapour continuum, *J. Atmos. Sci.*, 1974, 31, 255–260.

60. PRABHAKARA, C. AND DALU, G. — Remote sensing of the surface emissivity at 9 μm over the globe, *J. Geophys. Res.*, 1976, 81, 3719–3724.

61. PRABHAKRA, C., DALU, G. AND KUNDE, V. G. — Estimation of sea surface temperature from remote sensing in 11 to 13 μm window region, *J. of Geophys. Res.*, 1974, 79, 5039–5044.

62. SELBYM, J. E. A. AND MCCLATCHEY, R. M. — Atmospheric transmittance from 0·25 to 28·5 μm: computer code LOWTRAN-2, AFCRL-3572-0745, Environmental Research Paper no 427, Air Force Cambridge Research Laboratories (now Air Force Geophysical Laboratories), Bedford, Mass., 1972, 71 p.

63. COGAN, J. L. AND WILLAND, J. H. — Measurement of sea surface temperature by NOAA 2 satellite, *J. Appl. Meteorol*, 1976, 15, 173–180.

64. COGAN, J. L. — Interpretation of 8–13 μm measurements of sea-surface temperature. *Quart. J. Royal Meteorol. Socy.*, 1976, 102, 771–774.

65. SMITH, W. L., RAO, P. K., KOFLER, R. AND CURTIS, W. R. — The Deterimnation of Sea Surface Temperature from Satellite High Resolution Infrared Window Radiation measurements, *Mon. Wea. Rev.*, 1970, 98, 604–611.

66. ANDING, D. AND KATUH, R. — Estimation of sea surface temperature from space, *Remote Sensing of Environment*, 1970, 1, 217–220.

67. ANDING, D. AND KATU H, R. — Atmospheric modelling in the infrared spectral region : Atmospheric effects on multispectral sensing of sea-surface temperature from space. Report 2676–1–P, 1969. Willow Run Laboratories, Institute of Science and Technology, The University of Michigan, Ann Arbor, Michigan.

68. MAUL, G. A. AND SIDRAN, M. — Atmospheric effects on ocean surface temperature sensing from NOAA satellite scanning radiometer, *J. Geophys. Res.*, 1973, 78, 1909–1916.

69. COHEN, A. C. — Estimating the mean and standard deviation of truncated normal distributons, *J. American Statistical Association*, 1949, **44**, 518–525.

70. COHEN, A. C. — Estimating the mean variance of normal population from singly truncated and doubly truncated samples, *Annals of Mathematica l Statistics*, 1950, **21**, 557–569.

71. HALPERIN, M. — Estimation in the truncated normal distribution, *J. American Statistical Association*, 1952, 47, 457–465.

72. CROSBY, D. S. — Obtaining estimated clear radiances when some of the fields-of view are cloud contaminated, *Preprints of the Fourth Conference of Probability and Statistics in Atmospheric Sciences*, November 18–21, 1975, Tallahassee, Florida, pp. 163–164.

73. CROSBY, D. S. AND DEPRIEST, D. J. — Estimating clear column radiances : a report and a new decision rule, *Preprints of the Symposium on Remote Sensing*, Nov. 16–19, 1976, Melbourne, pp. 101–102.

74. KUMER, J. P. — Atmospheric CO_2 and N_2 vibrational temperatures at 40–140 km altitude, *J. Geophys. Res.*, 1977, 82, 2195–2202.

75. SMITH, W. L., WOOLF, H. M. AND FLEMING, H. E. — Retrieval of atmospheric temperature profiles from satellite measurements for dynamical forecasting, *J. Appl. Meteorol.*, 1972, **11**, 113–122.

76. MASON, B. J. — The contribution of satellites to the exploration of the global atmosphere and to the improvement of weather forecasting, *Measurement and Control*, 1973, 6, 441–451.